DETERMINATION OF PERMANENT MAGNET SYNCHRONOUS MOTOR PARAMETERS

LI WANG

DETERMINATION OF PERMANENT MAGNET SYNCHRONOUS MOTOR PARAMETERS

by

©Li Wang

A thesis submitted to School of Graduate
Studies in partial fulfillment of the
requirements for the degree of
Master of Engineering

Faculty of Engineering and Applied Science
Memorial University of Newfoundland

December 1989

St.John's Newfoundland Canada

ISBN 0-315-59216-8

Abstract

Permanent magnet (P.M.) excited synchronous machines have shown increasing popularity in recent years for industrial drive applications. However, the limitation imposed by permanent magnet excitation causes some difficulties in evaluating the machine parameters. This thesis presents the experimental procedure of the determination of the P.M. synchronous motor parameters. The work is intended to evaluate the d- and q-axis reactances and the permanent magnet generated voltage under load condition.

The air gap fields of the P.M. synchronous motor are evaluated for specific rotor and magnet configurations. An analog simulation of the interaction of these field quantities in the air gap is developed. A practical implementation of the digital measurement technique for determining motor torque angles is realized. A number of different test methods are developed and applied to a 3-phase, 60 Hz, 4-pole, 1 horsepower P.M. synchronous motor. Conventional test methods are modified for use on this type of the motor. A search coil test is developed to locate variation of the generated voltage with increasing load. The influence of the armature reaction is also investigated.

A flux linkage test is developed to measure the static inductance of the machine and the search coils inserted in the stator slots of the motor are used to measure air gap flux distribution. Calculation of the d- and q-axis reactances is based on the flux and the current measured. The measurement methods come from the transformation of the two-axis theory.

Contents

List of Tables

List of Figures

LIST OF SYMBOLS

a_0, a_n, b_n	Fourier coefficients
A_g	Area of air gap
A_m, A_{m1}, A_{m2}	Area of magnet section
B_f	Air gap flux density due to magnets
B_g	Air gap flux density
B_{f1}	Fundamental component of B_f
B_r	Residual flux density of magnets
B_{ad}, B_{aq}	Air gap flux density due to armature currents on the direct axis and quadrature axis
B'_1, B'_2	Operating flux density on magnet faces due to armature current only
B_{L1}, B_{L2},	Length of iron leakage paths, used for determining of armature reaction influence
d	Direct axis, used as subscript

D,	L_s,	Rotor dimensions
E,	E_i,	Voltage measured from air gap at different loading
E_0		Permanent magnet generated voltage
E_{max},	E_{min}	Maximum and minimum armature voltage in conventional test
E_{oc}		Open circuit voltage in conventional test
f		Frequency
F_{dm},	F_{qm}	Direct and quadrature armature mmfs
g		Equivalent air gap length
H		Magnetizing force
H_c		Coercive force of magnet material
H_f		Air gap magnetizing force due to magnets
H_g		Magnetizing force across air gap
H_t		Field strength in the bridge

H_1',	H_2'		Operating magnetizing force on magnet faces due to armature currents
h_1	h_2		Magnet dimensions
I			Current flow through the bridge circuit used in flux linkage test
I_a			Phase current
I_d,	I_q		Direct and quadrature axis currents
I_{fm}			Field current induced by magnets
I_{max},	I_{min}		Maximum and minimum armature current in conventional test
I_{sc}			Short-circuit current in conventional test
i_a,	i_b,	i_c	Armature current used in two-axis theory
i_d,	i_q,	i_0	Axes current used in two-axis theory
K,	K_l		Leakage factor
K_a,	K_b,	K_c	Gain of measurement circuit used in search coil test

K_w	Stator winding factor
K_1	Waveform factor for open circuit flux density waveform
L	Static inductance of the machine
L_1, L_2,	Length of the magnet section 1 and 2 in direction of flux
l_s	Length of the stator core
m	Number of stator phases
N	Number of stator series turns per phase
P	Number of poles
q	Quadrature axis used as subscript
R	Resistance or reluctance
R_g	Reluctance of air gap
R_m, R_{m1}, R_{m2}	Reluctance of magnets
R_l, $R_{l1,\ldots l4}$	Reluctance of leakage paths

R_1	Stator resistor
R_2, R_3, R_4	Resistor of measurement bridge in flux linkage test
T_e	motor torque
t_1, L_1	Leakage dimensions
V	rms value of applied stator voltage
V_{ab}	Voltage potential across the bridge used in flux linkage test
v_a, v_b, v_c	Stator voltage used in two-axis theory
v_d, v_q, v_0	Axes voltage used in two-axis theory
X_d, X_q	Direct and quadrature reactance
X_{md}	Direct magnetizing reactance
μ	Permeability of magnetic materials
S	Number of stator teeth
θ	Arbitrary angle between the two set of axes for two-axis theory. Angular displacement

θ_{ph}	Angular displacement between trapezoidal and sinusoidal components in analog simulation test
β	Geometrical factor for magnet leakage
δ	Torque angle
δ_0	Initial torque angle
ϕ	Power factor
Φ_f	Air gap flux
Φ_1	Peak amplitude of the flux
Φ_l, Φ_{l1}, Φ_{l2}	Leakage flux
Φ_m, Φ_{m1}, Φ_{m2}	Flux generated by magnets
Φ_r	Remanent flux
ψ	Flux linkage
ψ_d, ψ_q	Direct and quadrature axis flux linkage
ω	Angular frequency of alternating signal

ACKNOWLEDGEMENTS

The author wishes to express his sincere gratitude and appreciation to Professor T.A. Little for his valuable guidance, advice and financial support throughout the preparation of this thesis.

Financial support from the Memorial University of Newfoundland Graduate Student Bursary is highly appreciated as well.

Furthermore, the author wishes to thank all the friends of the Faculty of Engineering at Memorial University of Newfoundland for many useful discussions and suggestions. Appreciation is also expressed to the technicians for their help.

Finally, to my wife and daughter as well as my parents, without whose support, encouragement and understanding, this work would not have been completed, my sincere appreciation is expressed.

Chapter 1

INTRODUCTION

A significant technological change has occurred in motor drive systems in recent years, arising from the confluence of permanent magnet materials and semiconductor switching device technologies. One type of machine often used for these systems is the permanent magnet (hereafter abbreviated P.M.) excited synchronous motor. The P.M. synchronous motor offers several advantages over the d.c. excited synchronous motor. A primary advantage is that the P.M. motor does not need an external supply to excite the rotor field. Hence, the field winding and slip rings are eliminated. The absence of the field winding reduces the cost and eliminates the power loss associated with the field winding [1,2]. Moreover, the P.M. motor occupies less space than field windings for a given size, which leads to more compact designs [3]. It also minimizes maintenance.

Recent research has indicated that the P.M. synchronous motor has also become a serious competitor to the induction motor for high performance servo applications [4-7]. The P.M. synchronous motor is more efficient and has a larger torque to inertia ratio and power density when compared with the induction motor. In addition, for the same output capacity, the P.M. synchronous motor is smaller in size and lower in weight which makes it preferable for certain high performance application like robotics and aerospace actuators.

However, the P.M.synchronous motor has some disadvantages like other type of motors. One of these is the existence of a braking torque generated by the magnets during the starting period. This decreases the motor's ability to synchronize a load [8-9]. The problem can be reduced by designing a cage winding having a high resistance to provide sufficient accelerating torque.

In order to understand the basic characteristic of the P.M. synchronous motor, it is necessary first to appreciate the distinguishing configuration of the interior P.M. motor itself. The following description is appropriate only to interior P.M. motor where magnets are mounted inside the rotor. By using the sample four-pole rotor geometry shown in Fig.1.1, the magnetic flux produced by magnets defines a direct-axis radially through the centerline of the magnets. An orthogonal quadrature-axis is defined through the interpolar region separated from the d-axis by 45 mechanical degrees (i.e. 90 electrical degrees for a four-pole design). As sketched in Fig.1.1, the magnetic flux passing through the d-axis magnetic circuit must cross two magnet thicknesses. Since the incremental permeability of P.M. materials (ceramic, rare-earth, etc) is nearly that of free space, the magnet thickness appear as large series air gaps in the d-axis magnetic flux paths. Since the q-axis magnetic flux can pass through the steel pole pieces without crossing the magnet air gap, the q-axis reactance is noticeably higher than that of the d-axis. This introduces a saliency into the rotor magnetic circuit in which the q-axis reactance is larger than the d-axis reactance. In contrast, the conventional wire-wound synchronous motor has a value of X_q which is normally 60 - 70% of the value of X_d for the salient pole rotor machine. Different design of rotor configuration and geometry provides different values for the ratio X_d/X_q, which will alter the torque production and performance of the P.M. synchronous motor during both steady state operation and the run-up period [10-13].

The values of X_d and X_q for the conventional synchronous motor can be measured by standard test procedures [14]. However, these procedures are not suitable for P.M. synchronous motor because of its permanent excitation. Thus, available experimental

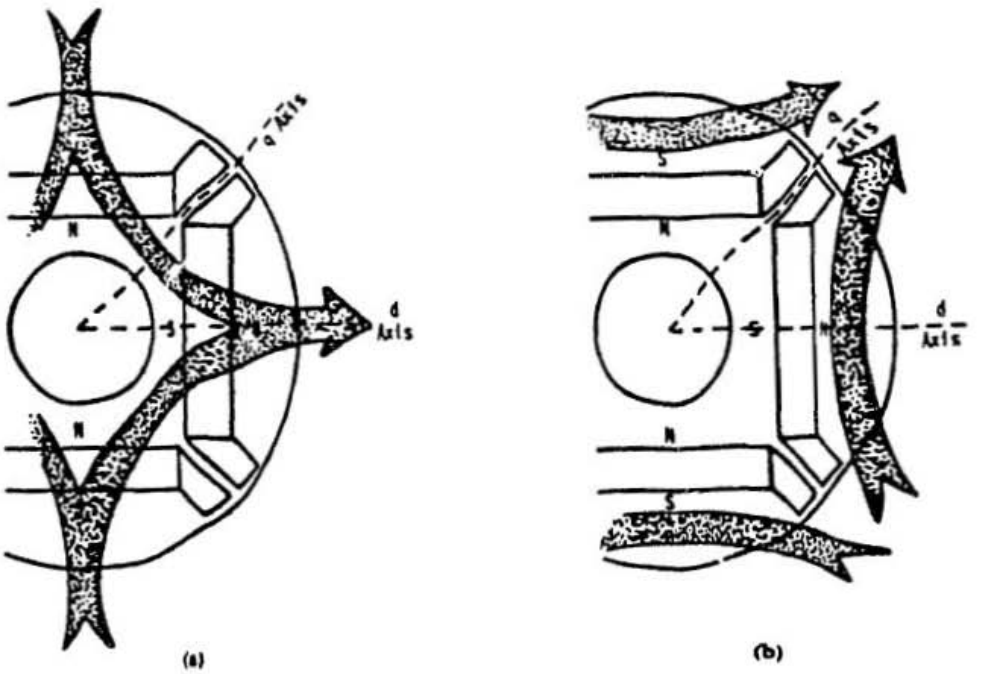

Figure 1.1: Principal magnetic flux paths: a) d-axis, b) q-axis

methods by which the P.M. machine parameters can be evaluated accurately have been a subject of many investigators. This research is intended to determine the d- and q- axis reactances and permanent magnet generated voltage of P.M. synchronous motor.

An outline of the remaining chapters of this thesis is given as follows:

Chapter 2 presents conventional tests for synchronous motors and introduces the basic characteristics of the P.M. synchronous motors and three of the important motor parameters. A literature review dealing with the measurement of these parameters is also presented.

An evaluation of the air gap fields of the P.M. synchronous motor follows in Chapter 3. An analog simulation of the interaction between these field quantities in the air gap is shown and a digital measurement technique for determining the motor torque angle is also developed.

The measurement of the machine reactance parameters is presented in Chapter 4 and 5. A number of different test methods are shown and the analysis for each method is given. Conventional test methods are modified for use on the P.M. synchronous motor.

Finally, Chapter 6 presents the conclusions of this research work. Suggestions for further study are also given.

Chapter 2

BASIC CHARACTERISTICS OF P.M. SYNCHRONOUS MOTORS

2.1 Introduction

A general introduction to the P.M. synchronous motor was presented in the last chapter. It was shown that permanent excitation of the P.M. synchronous motor results in some differences when compared with d.c. excited synchronous motors. Consequently, conventional tests for the synchronous motor cannot be applied to the P.M. synchronous motor and alternate test methods must be devised to determine its characteristics and parameters.

In order to understand the difference in test methods between the conventional and the P.M. machines, the tests for conventional synchronous motor are introduced first. Then the reasons of why these tests cannot be applied to the P.M. machines are presented. Finally the literature covering the determination of P.M. synchronous motor parameters is reviewed.

2.2 Conventional Test for Synchronous Motors

There are two different types of synchronous machine due to different rotor structures, one being a cylindrical- and the other being a salient-pole synchronous machine. A typical salient-pole rotor structure is shown in Fig.2.1. It is clear that the air gap is much larger on the quadrature-axis (i.e. in the interpolator space) than on the direct-axis. Since the air gap is of minimum length in the direct-axis, a given armature mmf directed along that axis produces a maximum value of flux. The same armature mmf directed along the quadrature-axis, where the air gap has its greatest length, produces a minimum value of flux. The synchronous reactance associated with the direct- axis is therefore a maximum and is known as the d-axis synchronous reactance X_d, the minimum synchronous reactance is called the q-axis synchronous reactance X_q.

The conventional way of determining machine parameters is defined by "Test Procedures of Synchronous Machines" [14], which includes the open-circuit and short-circuit test, slip test, etc and will be introduced as follows.

2.2.1 Open-Circuit and Short-Circuit Test

This is a way of determining X_d from the measurement of the steady-state armature open-circuit voltage and short-circuit current [15-16]. The rotor of the machine is driven at rated speed with the field winding excited, and the open circuit armature voltage measured. A three-phase short circuit is applied to the armature terminals and the sustained armature current is measured, keeping the field current constant. The direct-axis reactance may be found from the ratio of the open-circuit voltage to the short-circuit current. If the machine is saturated, the voltage read from the open-circuit line should be used instead of the air gap line. The result is the saturated value of X_d, see Fig.2.2.

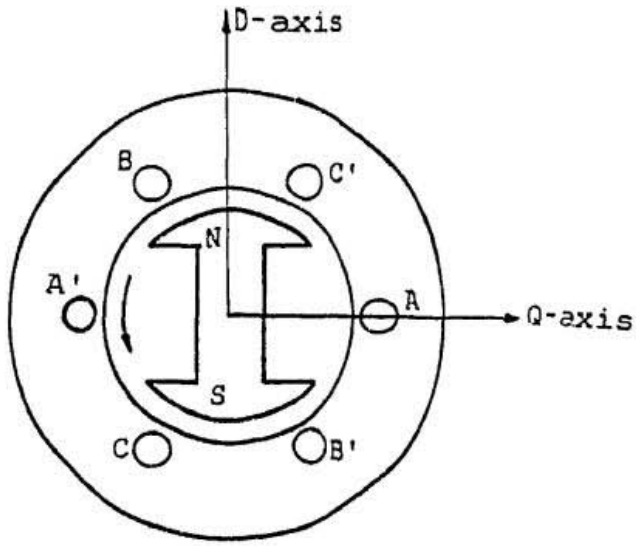

Figure 2.1: Rotor structure of the salient-pole machine

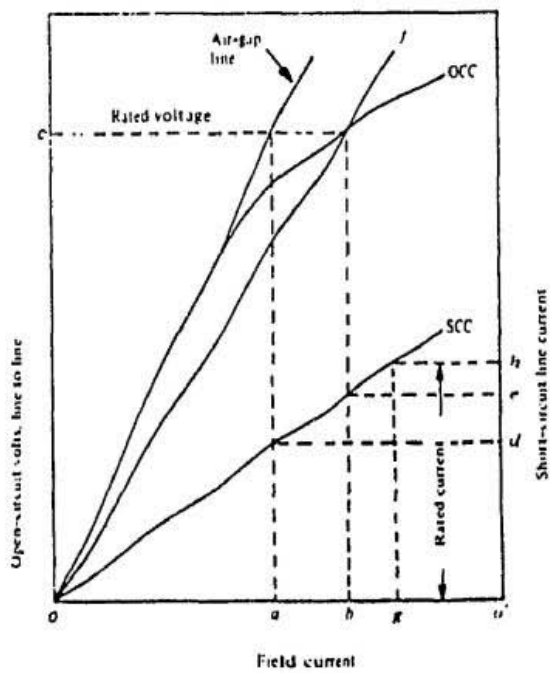

Figure 2.2: Open-circuit and short-circuit test

$$X_d = \frac{oc}{\sqrt{3}o'd} \ (unsaturated) \tag{2.1}$$

or

$$X_d = \frac{oc}{\sqrt{3}o'e} \ (saturated) \tag{2.2}$$

2.2.2 Slip Test

The slip test is carried out by applying a reduced, balanced, three-phase voltage at rated frequency to the stator, while the rotor is driven at a speed very slightly different from synchronous speed with the field circuit open [14-15]. The phase sequence of the applied voltage must be such that the armature mmf and the rotor travel in the same direction. The d-axis and q-axis of the rotor thus alternately slips past the axis of the armature mmf, causing the armature mmf to react alternately along the direct and quadrature axes. The armature current, and voltage, as well as the voltage across the open circuit field winding are observed. The measurement method and a typical oscillogram are shown in Fig.2.3. The minimum and maximum ratio of the armature voltage to the armature current are obtained when the slip is very small. For these, approximate values of d-axis and q-axis synchronous reactance can be obtained by the following equations:

$$X_d = \frac{E_{max}}{I_{min}} \ per \ unit \tag{2.3}$$

$$X_q = \frac{E_{min}}{I_{max}} \ per \ unit \tag{2.4}$$

The reactance X_q is less than the reactance X_d because of the greater reluctance of the air gap on the quadrature axis. Usually X_q is between $0.6X_d$ and $0.7X_d$.

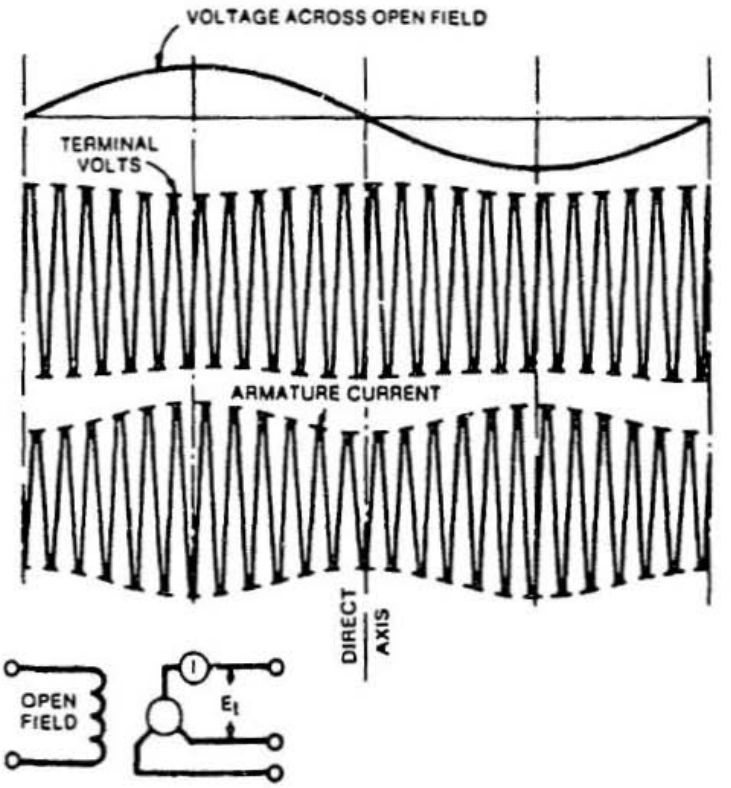

Figure 2.3: Slip test

2.3 Basic Characteristics of The P.M. Synchronous Motor and Its Parameters

There are three critical parameters for P.M. synchronous motor from which the steady-state performance of the machine can be determined [11,17-18].

$$\begin{aligned} T_e &= \frac{3}{\omega}[\frac{E_0 V}{X_d} sin\,\delta - \frac{V^2}{2}(\frac{1}{X_d} - \frac{1}{X_q}) sin\,2\delta] \\ &= T_1 sin\,\delta - T_2 sin\,2\delta \end{aligned} \tag{2.5}$$

In equation (2.5), E_0 is the permanent magnet generated voltage and is equal to the product $X_{md} * I_{fm}$, where X_{md} is the direct axis magnetizing reactance and I_{fm} is the field current induced by magnet flux, while X_d and X_q are the synchronous reactance in the d-axis and the q-axis which are similar to those of conventional synchronous motors. Testing and characterization of the P.M. synchronous motor are in principle similar to the procedures applied to the conventional synchronous motor. However, there are three characteristic features of the P.M. motor which result in some difficulties in using conventional test procedures on the P.M. synchronous motor [19]. The tests which are particularly affected are those from which X_d and X_q can be obtained. These relevant features of the P.M. synchronous motor are:

- The motor is permanently excited;
- X_d is generally appreciably less than X_q;
- The reactance parameters are more sensitive to saturation effects than those of the conventional machine.

Firstly, permanent excitation makes it difficult to employ the conventional slip test as a means for determining X_q. Open-circuit and short-circuit tests have to be modified as well to be applied to the P.M. synchronous motor (hereafter called

"modified conventional test"). Secondly, since X_d is less than X_q, the second term in equation (2.5) is opposite in sign to that obtained in the conventional synchronous motor. Because of this, the peak torque for the P.M. motor occurs at an angle larger than 90^0. If the difference between d- and q-axis reactances is large enough, the torque at small torque angles becomes negative. This means that the torque angle at no load is larger than zero (This will be verified practically during the no-load test). Finally, the effects of saturation cause the machine parameters to vary with load. Subsequently, alternate test methods must be devised to locate the machine parameters.

Simply X_d and X_q can be found from the steady state voltage equations of the P.M. synchronous motor [18], which are given as follows:

$$X_d = \frac{V\cos\delta - E_0}{I_a \sin(\phi - \delta)} - \frac{R_1 I_a \cos(\phi - \delta)}{I_a \sin(\phi - \delta)} \tag{2.6}$$

$$X_q = \frac{V\sin\delta}{I_a \cos(\phi - \delta)} + \frac{R_1 I_a \sin(\phi - \delta)}{I_a \cos(\phi - \delta)} \tag{2.7}$$

where:

V: applied voltage

E_0: open circuit voltage

I_a: phase current

R_1: stator resistance

ϕ: power factor

δ: torque angle

It should be noted here that the determination of X_d involves internal generated voltage which is assumed to be equal to the open circuit value E_0 and remains constant. However, E_0 in practice, is a quantity which varies with the load. The open circuit

voltage may be found from the expression [20]:

$$E_0 = \frac{2\pi}{\sqrt{2}} f \Phi_1 N K_w \times 10^{-8} \tag{2.8}$$

or

$$E_0 = \frac{4}{\sqrt{2}} f K_1 B_f A_g N K_w \times 10^{-8} \tag{2.9}$$

The following expression can be obtained by substituting $B_f = \frac{B_r(A_m/A_g)}{1+\beta K_l}$ into Eq.(2.9):

$$E_0 = \frac{4}{\sqrt{2}} f K_1 A_g N K_w \frac{B_r(A_m/A_g)}{1+\beta K_l} \times 10^{-8} \tag{2.10}$$

Since the open circuit voltage E_0 involves the leakage factor K=1+βK_l which varies with the stator current under load condition, Thus E_0 is a machine-saturable parameter which depends on the saturation of the steel leakage bridges. Consequently, X_d is also a quantity affected by saturation. To determine E_0, it may be measured only as an open circuit quantity. It is impossible to measure the open- and short-circuit characteristic in the usual way because the excitation cannot be varied. Neither can X_d and X_q be measured by the slip test, because this requires the excitation to be removed.

2.4 Review of Literature

With regard to the determination of P.M. synchronous machine parameters, the literature of the recent years has been divided into two different types. The first and largest group has been concerned with computational methods for determining the significant parameters of the machine. The second group, which has a much smaller following has dealt with the test aspect of being able to measure the machine parameters.

The computational methods use some numerical iterative procedure to solve the magnetic field of the machine given some specific geometry. Of the various methods available the finite-element method is the most commonly reported, see references [22-27]. Other methods for solving the nonlinear magnetic field equations by iterative methods have been presented, see references [3,17,21,28]. Among them, V.B. Honsinger [21] has presented a critical work. The method presented allows the determination of the saturated values of the machine parameters and the work is quite well for predicating motor performance at entire range of loads. These methods which provide relatively accurate models at the expense of significant computational effort, are primarily aimed at design work and are less concerned with the actual measurement of parameters. Moreover, for these kind of methods complete knowledge values of internal construction of the machine is required and is usually not available.

Without the ability to remove field excitation from P.M. synchronous machine, the conventional methods of electrical parameters identification cannot be utilized. Consequently, a quite limited reporting of measurement of machine parameters is available in the literature. The most significant works dealing with the actual measurement of parameters have come from General Electrics motor development laboratories and of whom T.J.E. Miller and V.B. Honsinger [19,21] have been the principle characters. Honsinger has presented several modified conventional tests which can be used to measure motor parameters. This method allows the measurement of both unsaturated and saturated values of machine parameters and work is suitable for predicting motor performance at no-load and heavy load conditions. Miller has presented a method for static determination of the machine axis inductances. His methods are based on an earlier work by C.V. Jones [29] and incorporate the interaction of d-q axis flux. Miller also presented a load test to measure the X_d and X_q. His results clearly show that there is a region near zero d-axis current where the d-axis inductance varies significantly.

In load test provided by Miller [19], a set of data has to be measured including

machine torque angle. Most existing measurement devices for measuring torque angle use a stroboscope and a graduated disc affixed on the stator frame. This kind of measurement has poor resolution and is not convenient to use in practical tests. Moreover, it cannot meet the requirement of the machine drive system where all the parameters have to acquired electronically and digitally, references [30-31].

In end of the references cited above, although mention was made of the variation of the generated voltage, E_0, all of the calculation were done under the assumption of constant E_0. Consequently, saturated value of X_d presented by Honsinger [21] must be considered as a approximate value. The agreement between load test and static inductance measurement presented by Miller [19] is also less than satisfactory. It is the objective of this work to investigate this variation more thoroughly, to validate the various test methods and to incorporate a digital technique for measuring torque angle.

Chapter 3

FIELDS OF P.M. SYNCHRONOUS MOTORS

3.1 Introduction

In order to determine the machine parameters, the air gap fields of the machine must be known. The objectives of this chapter is to develop air gap field descriptions based on the configuration of the motor with radially oriented and inset magnets. Moreover, the interaction of the field quantities in the air gap is verified by analog circuit simulation. The results of this simulation is employed to measure the motor torque angle by digital techniques.

3.2 Air Gap Fields

Air gap field of the P.M. synchronous machine can be described by a consideration of the configuration of the rotor and magnetic circuit of the machine. There are two flux sources contributing to the air gap field in the P.M. synchronous machine. One is produced by the magnets in the rotor. The other is generated by the stator current. The flux density distribution in the air gap is the resultant of these two flux

components, each of which will be discussed separately in the following sections. The field models and analy ,is based on Honsinger's research [21] are given first. The work is extended to develop an analog circuit to simulate the field models and a digital circuit to measure the motor torque angles. Figure 3.1 and figure 3.2 show rotor and magnet configuration used in this study and the various paths available to the magnet flux. Since the magnets in the rotor lie in the direct-axis of the machine, the magnets will influence the d-axis field, without affecting the q-axis field.

3.2.1 Magnet Fields

Six equations are used to describe the magnet fields due to the P.M. acting alone:

$$B_1 = -\mu_1' H_1 + B_{r1} \tag{3.1}$$

$$B_2 = -\mu_2' H_2 + B_{r2} \tag{3.2}$$

$$\Phi_m = \Phi_f + \Phi_l \tag{3.3}$$

$$H_1 L_1 - 2 H_2 L_2 = 0 \tag{3.4}$$

$$2 g H_f - H_1 L_1 = 0 \tag{3.5}$$

$$\Phi_l = 2 \frac{\Phi_f R_g}{R_l} \tag{3.6}$$

Equations (3.1) to (3.6) are based on the rotor configuration shown in figure 3.1 and flux paths shown in Figure 3.2 as well the magnet characteristic as shown by figure 3.3. In this work, the analysis is applicable for various magnet materials and requires a rotor construction with radially oriented and inset magnets. This is the most common design of P.M. synchronous motors. The derivation of this set equation is shown as follows.

1. Model of The Magnetic Materials

Considering the rotor construction shown in Fig.3.1, it is clear that there are two magnet sections in the rotor contributing to the total air gap flux. The basic

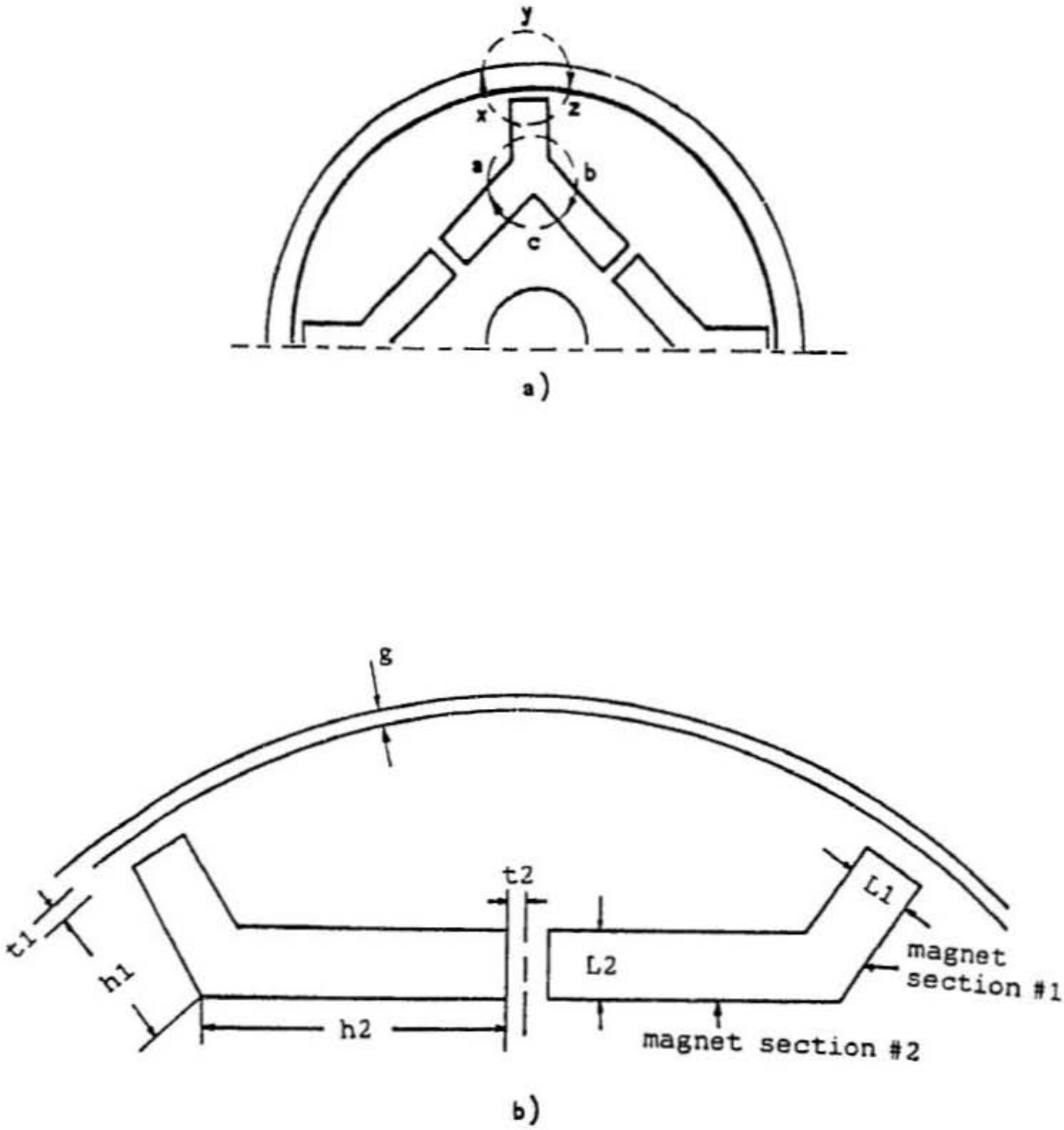

Figure 3.1: Rotor and magnet geometry: a) rotor and magnet configuration b) dimensions

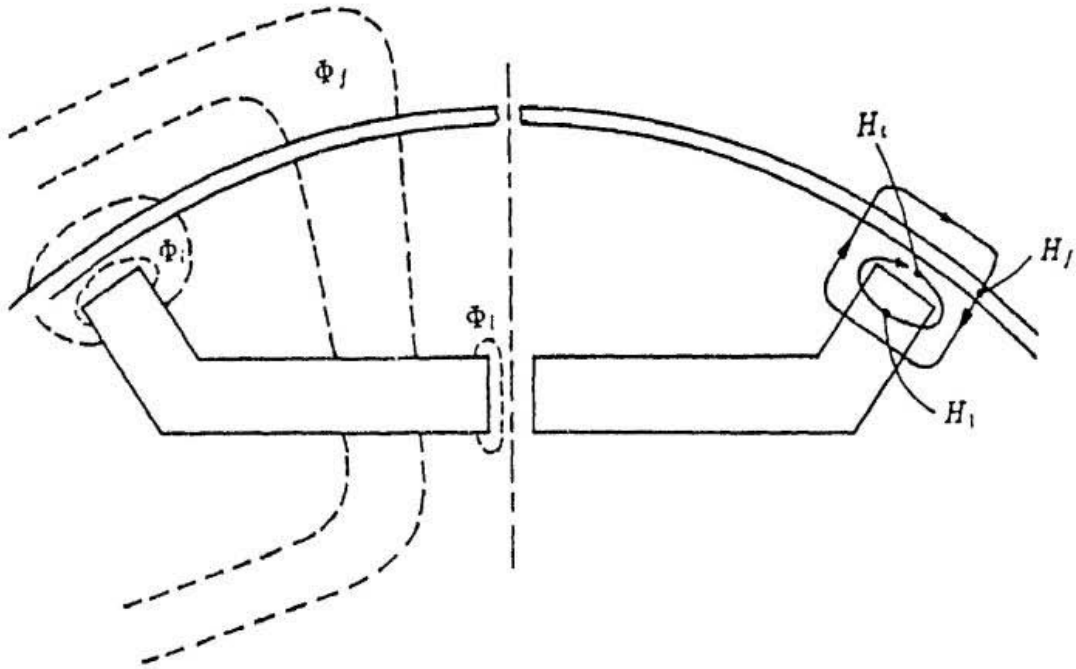

Figure 3.2: Flux paths of the magnets

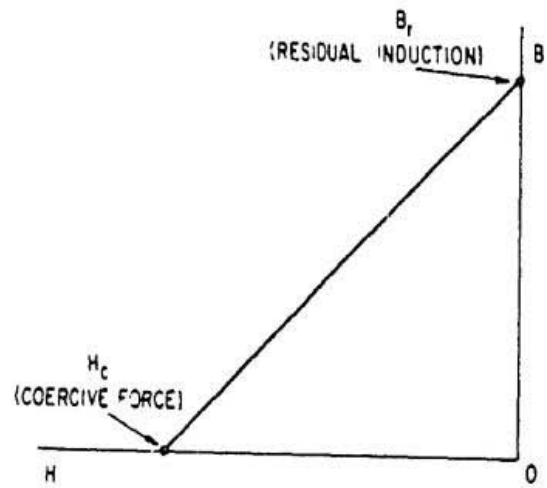

Figure 3.3: BH characteristic of the magnet materials

demagnetization curve of the permanent magnet material in these sections may be modeled as:

$$B = -\mu' H + B_r \tag{3.7}$$

where slope μ' is equal to: $+B_r / H_c$. Therefore, the recoil BH characteristic of the magnet is written as follows for magnetic section 1 and section 2:

$$B_1 = -\mu_1' H_1 + B_{r1} \tag{3.8}$$

$$B_2 = -\mu_2' H_2 + B_{r2} \tag{3.9}$$

2. Flux Balance Equation

The flux Φ_m created by the two magnets is equal to the sum of the magnet air gap flux Φ_f and the steel bridges leakage flux Φ_l, and may be written as:

$$\Phi_m = \Phi_f + \Phi_l \tag{3.10}$$

or

$$\Phi_f = \Phi_m - \Phi_l \tag{3.11}$$

where

$$\begin{aligned} \Phi_m &= \Phi_{m1} + \Phi_{m2} \\ &= B_1 A_{m1} + B_2 A_{m2} \\ &= 2 l_s (h_1 B_1 + h_2 B_2) \end{aligned} \tag{3.12}$$

and Φ_l will be given later.

3. Applying Ampere's circuital law to the two flux paths: path xyz crosses the air gap into the stator to link the stator winding, while path abc is located entirely in the rotor and links only the rotor magnets. Thus, the equation based on Ampere's circuital law may be written as (for paths abc and xyz respectively):

$$H_1 L_1 - 2 H_2 L_2 = 0 \tag{3.13}$$

$$2 g H_f - H_1 L_1 = 0 \tag{3.14}$$

The vector direction for the H and B fields is opposite in sign for the magnet material but is of the same sign in the air gap.

4. Leakage Flux in The Steel Bridges

The leakage flux in the steel bridges is dependent upon the combination of the magnet mmf and the armature mmf. In order to calculate the leakage flux, the following is assumed.

- stator winding is open-circuited, in which case stator current is zero, thus there is no armature reaction;
- permeability in the iron is infinite everywhere except in the steel bridges surrounding the magnets.

By considering the outer bridge, Ampere's Law results in:

$$H_1 L_1 - H_{t1} L_1 = 0 \tag{3.15}$$

$$2g H_f - H_1 L_1 = 0 \tag{3.16}$$

Combining the above equations, gives,

$$H_{t1} = \frac{2g H_f}{L_1} \tag{3.17}$$

Thus, the bridge flux density is:

$$\begin{aligned} B_{t1} &= \mu_1 H_{t1} \\ &= \frac{\mu_1 2g H_f}{L_1} \end{aligned} \tag{3.18}$$

The leakage flux for two such bridges (per pole) is:

$$\begin{aligned} \Phi_{t1} &= B_{t1} 2t_1 l_s \\ &= \frac{2\Phi_f R_g}{R_{t1}} \end{aligned} \tag{3.19}$$

where $\Phi_f = B_f A_g$

$R_g = \frac{g}{A_g}$

$R_{l1} = \frac{L_1}{2 u_1 t_1 l_s}$

The total leakage flux per pole is :

$$\begin{aligned} \Phi_l &= \Phi_{l1} + \Phi_{l2} \\ &= 2\Phi_f \frac{R_g}{R_l} \end{aligned} \tag{3.20}$$

where $R_l = \frac{1}{2l_s(\frac{u_1 t_1}{L_1} + \frac{u_2 t_2}{L_2})}$

5. The Flux Density in The Air Gap

A set of equations Eq.(3.1) - Eq.(3.6) has been set up to give a description for the magnet fields. The flux density in the air gap produced by the magnets will be derived from these equations. The derivation is as follows. Substituting Eq.(3.1) and Eq.(3.2) into Eq.(3.3) and rearranging, gives,

$$\Phi_r - 2l_s(h_1 \mu_1' H_1 + h_2 \mu_2' H_2) = \Phi_f + \Phi_l \tag{3.21}$$

where $\Phi_r = 2l_s(h_1 B_{r1} + h_2 B_{r2})$ is the remanent flux

From Eq.(3.4) and Eq.(3.5), gives,

$$H_1 = \frac{2g H_f}{L_1} \tag{3.22}$$

$$H_2 = \frac{2g H_f}{2L_2} \tag{3.23}$$

Substituting Eq.(3.6), Eq.(3.22) and Eq.(3.23) in Eq.(3.21), yields,

$$\Phi_r - 2g H_f(\frac{2l_s h_1 \mu_1'}{L_1} + \frac{2l_s h_2 \mu_2'}{2L_2}) = \Phi_f(1 + 2\frac{R_g}{R_l}) \tag{3.24}$$

Letting

$$R_1 = \frac{L_1}{2 l_s h_1 \mu_1'} \tag{3.25}$$

$$R_2 = \frac{L_2}{2 l_s h_2 \mu_2'} \tag{3.26}$$

and substituting them into Eq.(3.24), the following is obtained:

$$\Phi_r - 2\Phi_f R_g \left(\frac{1}{R_1} + \frac{1}{2 R_2} \right) = \Phi_f \left(1 + 2 \frac{R_g}{R_l} \right) \tag{3.27}$$

where $\Phi_f R_g = H_f g$

Solving Eq.(3.27) for the air gap flux Φ_f, gives,

$$\Phi_r = \Phi_f \left[\left(1 + 2 \frac{R_g}{R_l} \right) + 2 R_g \left(\frac{1}{R_1} + \frac{1}{2 R_2} \right) \right] \tag{3.28}$$

Thus,

$$\Phi_f = \frac{\Phi_r}{1 + 2 \frac{R_g}{R_l} + 2 R_g \left(\frac{1}{R_1} + \frac{1}{2 R_2} \right)} = \frac{\Phi_r}{1 + \beta K_l} \tag{3.29}$$

where

$R_m = \frac{1}{\frac{1}{R_1} + \frac{1}{2 R_2}}$

$\beta = \frac{2 R_g}{R_m}$

$K_l = 1 + \frac{R_m}{R_l}$

Φ_f: air gap flux

Φ_r: remanent flux

The equation (3.29) states that the total residual flux of the magnet Φ_r is reduced by the machine geometry β and the leakage flux K_l. Rearranging of Eq.(3.29) with

$\Phi_r = B_r A_m$, yields

$$\begin{aligned} \Phi_f &= \frac{B_r A_m}{1 + \beta K_l} \\ &= B_r A_g \frac{A_m / A_g}{1 + \beta K_l} \end{aligned} \tag{3.30}$$

Hence, flux density in the air gap is given by

$$\begin{aligned} B_f &= \frac{\Phi_f}{A_g} \\ &= \frac{B_r (A_m / A_g)}{1 + \beta K_l} \end{aligned} \tag{3.31}$$

This is the flux density caused by the magnets acting alone. The flux density waveform described by Eq.(3.31) is a trapezoidal waveform and shown in Fig.3.1.

3.2.2 Armature Fields

The air gap field caused by the armature current acting alone has a d-axis component and a q-axis component. As stated at the beginning of this section, the magnets in the rotor are located on the d-axis of the machine, therefore both the magnets and the armature winding contribute to the d-axis flux. The stator currents are the sole source of flux on the q-axis. This special feature will be considered in the following analysis of the armature field.

1). Direct-Axis Field Caused by Stator Currents

A set of equation are defined to describe direct axis armature fields:

$$H_1' L_1 - 2 H_2' L_2 = 0 \tag{3.32}$$

$$2g H_{ad} + H_1' L_1 = 0.8 \pi F_{dm} \cos(\frac{P}{2})\theta \tag{3.33}$$

$$\Phi_{ad} = \Phi_m' + \Phi_l' \tag{3.34}$$

$$B_1' = \mu' H_1' \tag{3.35}$$

$$B_2' = \mu' H_2' \tag{3.36}$$

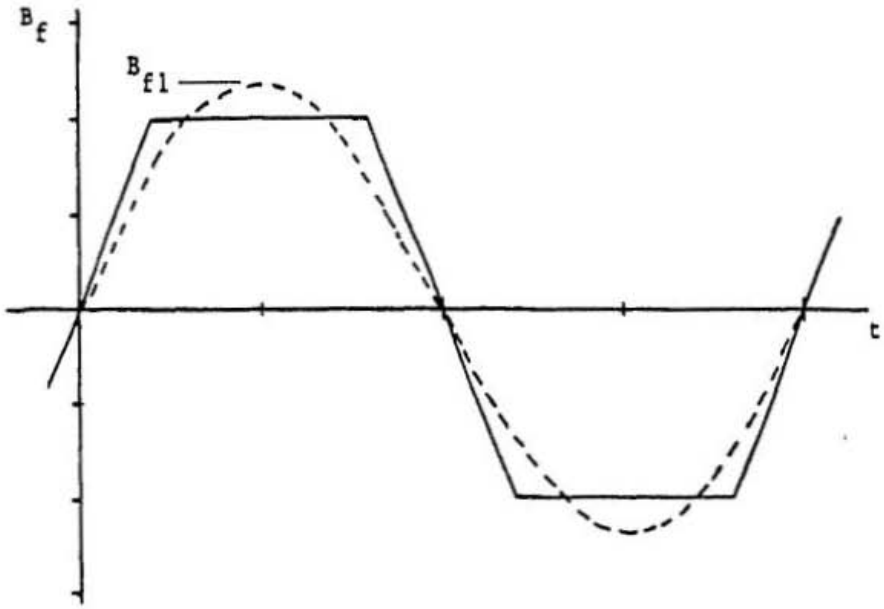

Figure 3.4: Flux density due to the magnets

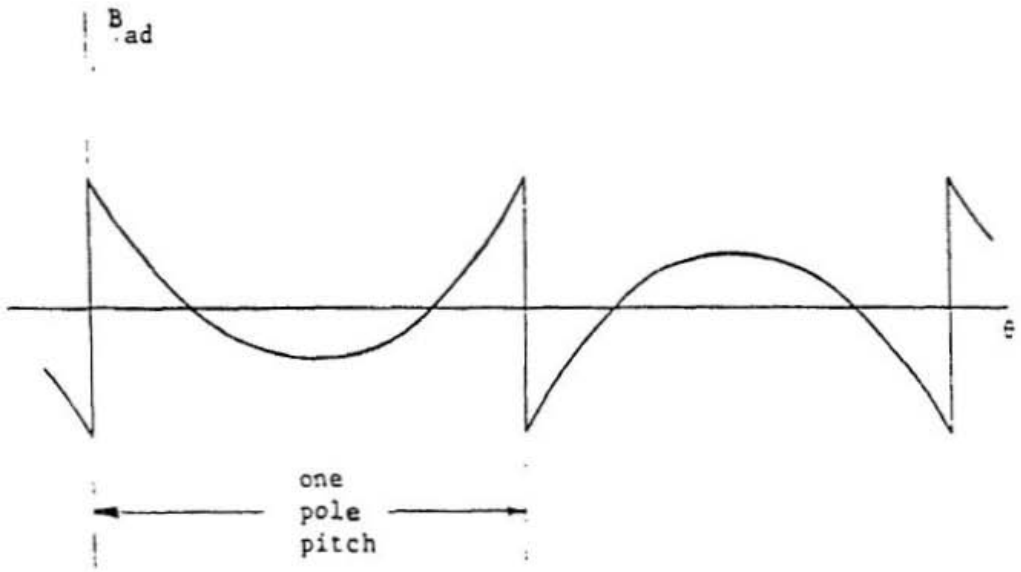

Figure 3.5: Direct-axis field due to the armature current

Eq.(3.32) to Eq.(3.36) are obtained from Eq.(3.1) to Eq.(3.6) with some exceptions as follows:

- The circuit equation for path xyz encloses an amount of the stator current given by $(2\ F_{dm}\ \cos(p/2)\theta)$ which is sole source of the flux.
- The magnets are unmagnetized, in which case the magnet has zero remanent magnetism.
- The flux balance equation changes its form to: $\Phi_{ad} = \Phi'_m + \Phi'_l$.

In the above equations, Φ_{ad} is the flux which crosses the air gap and can be determined by integrating the d-axis flux field B_{ad} over one pole pitch:

$$\begin{aligned} \Phi_{ad} &= \int_{-\pi/p}^{\pi/p} B_{ad}\, r\, d\theta \\ &= D\, L_s \int_0^{\pi/p} B_{ad}\, d\theta \end{aligned} \tag{3.37}$$

Hence, the flux balance equation is rewritten as:

$$\begin{aligned} D\, L_s \int_0^{\pi/p} B_{ad}\, d\theta &= \Phi'_m + \Phi'_l \\ &= \Phi'_m\, K_l \end{aligned} \tag{3.38}$$

where $K_l = 1 + \frac{\Phi'_l}{\Phi'_m}$

The flux generated by the two magnet sections is given previously by:

$$\Phi'_m = 2\, L_s\, (h_1\, B_1 + h_2\, B_2) \tag{3.39}$$

Substituting Equations (3.32), (3.35) and (3.36) into Eq.(3.39), gives,

$$\begin{aligned} \Phi'_m &= 2\, L_s\, (h_1\, \mu'\, H'_1 + h_2\, \mu'\, H'_2) \\ &= H'_1\, L_1\, (\frac{1}{R_1} + \frac{1}{2\, R_2}) \\ &= \frac{H'_1\, L_1}{R_m} \end{aligned} \tag{3.40}$$

where R_1, R_2 and R_m have been given previously. The integration of equation (3.37) is performed by substituting the value of B_{ad} from equation (3.33) where $B_{ad} = \mu_0 H_{ad}$.

$$\begin{aligned} D L_s \int_0^{\pi/p} B_{ad}\, d\theta &= D L_s \mu_0 \int_0^{\pi/p} H_{ad}\, d\theta \\ &= D Ls \mu_0 \int_0^{\pi/p} \left(\frac{0.8}{2g} F_{dm} \cos \frac{P}{2}\theta - \frac{H_1' L_1}{2g} \right) d\theta \\ &= \mu_0 \frac{1}{2R_g} (1.6 F_{dm} - H_1' L_1) \end{aligned} \tag{3.41}$$

where:

$R_g = \frac{g}{A_g}$: air gap reluctance

$A_g = \frac{D L_s}{P}$: area of air gap

Substituting equation (3.41) and (3.40) in equation (3.38), gives,

$$H_1' = \frac{1.6 \mu_0 F_{dm}}{L_1 (1 + \beta K_f)} \tag{3.42}$$

where: $\beta = 2 \frac{R_g}{R_m}$, given previously.

The air gap flux density B_{ad} can now be found from Eq.(3.33) by eliminating H_1' which is given in Eq.(3.42), and results in:

$$B_{ad} = \frac{0.4 \mu_0 \pi F_{dm}}{g} \left[\cos \frac{P}{2}\theta - \frac{2\mu_0 / \pi}{1 + \beta K_f} \right] \tag{3.43}$$

It is observed that the d-axis field described by Eq.(3.43) includes two components, one being a sinusoidal term and the other being a trapezoidal term, and the composite waveform is shown in Fig.3.5.

2). Quadrature-Axis Field Caused by Armature Currents

The q-axis flux density B_{aq} is similar to the d-axis flux density B_{ad} except for components related to the magnets and is given by the expression:

$$B_{aq} = \frac{0.4\mu_0 \pi F_{qm}}{g} \sin \frac{P}{2}\theta \tag{3.44}$$

3.2.3 Air Gap Fields

Up to now, three primary equations have been obtained which now can be used to describe the air gap fields of the P.M. synchronous motor. The three equations are repeated here for convenience:

$$B_f = \frac{B_r(A_m/A_g)}{1+\beta K_l} \tag{3.45}$$

$$B_{ad} = \frac{0.4\mu_0 \pi F_{dm}}{g}\left[\cos\frac{P}{2}\theta - \frac{2\mu_0/\pi}{1+\beta K_l}\right] \tag{3.46}$$

$$B_{aq} = \frac{0.4\mu_0 \pi F_{qm}}{g} \sin \frac{P}{2}\theta \tag{3.47}$$

Based on the analysis given above, it is clear that the flux density in the air gap is composed of a magnet field and an armature current field which may be written as:

$$B_g = f(B_f, B_{ad}, B_{aq}) \tag{3.48}$$

It has been stated that of these components the magnet component is constant over one pole pitch and has a trapezoidal waveform. The waveform of d-axis armature current component is the resultant of sinusoidal and trapezoidal terms; while the q-axis armature current component may be described by a purely sinusoidal waveform. The analysis of the air gap fields as described above results in following comments. Firstly, an analog simulation can be implemented to simulate various components in the air gap and their interaction from which it will be shown whether this field model gives a reasonable description to actual field of the machine. Secondly, it provides an analytical expressions to investigate influence of the armature reaction on generated

voltage at load conditions which will be of significant meaning as predicating steady-state performance of the machine by use of the load test. Both of these will be realized in this work.

3.3 Analog Simulation of The Fields

Based on the results of the preceding analysis, a simulation circuit may be developed to help understand the air gap field described in the last section. The simulation circuit is composed of a signal source, waveform shaping circuit and phase shifter. A block diagram of the circuit is shown in Fig.3.6 and the circuit is shown in Appendix *I*. The signal generator provides two types of signals, sinusoidal and triangular where the the triangular is used to form a trapezoidal signal which represents the magnet generated voltage by use of a waveform shaping circuit. The output of the subtract circuit in which inputs are the sinusoidal and trapezoidal signals, is used to represent the flux in the d-axis. The output of the phase shifter is used to represent the flux in the q-axis. These three signals, representing B_{ad}, B_f and B_{aq} respectively, are synthesized in the summation circuit to simulate the air gap flux B_g, in which operation is based on the assumptions given by:

$$B_g = B_f + B_{ad} + B_{aq} \tag{3.49}$$

With different angular displacement between B_{ad} and B_f, the results of simulation are shown in Fig.3.7. Strictly speaking, the fields in the air gap cannot be obtained by a linear synthesis of the three components. The reason for this is that the rotor iron is magnetically nonlinear and the leakage flux in the steel bridges surrounding the magnets is nonlinearly dependent on the loading condition.

However upon comparing the results of the simulation and the actual air gap flux waveform of figure 3.8, it is clear that:

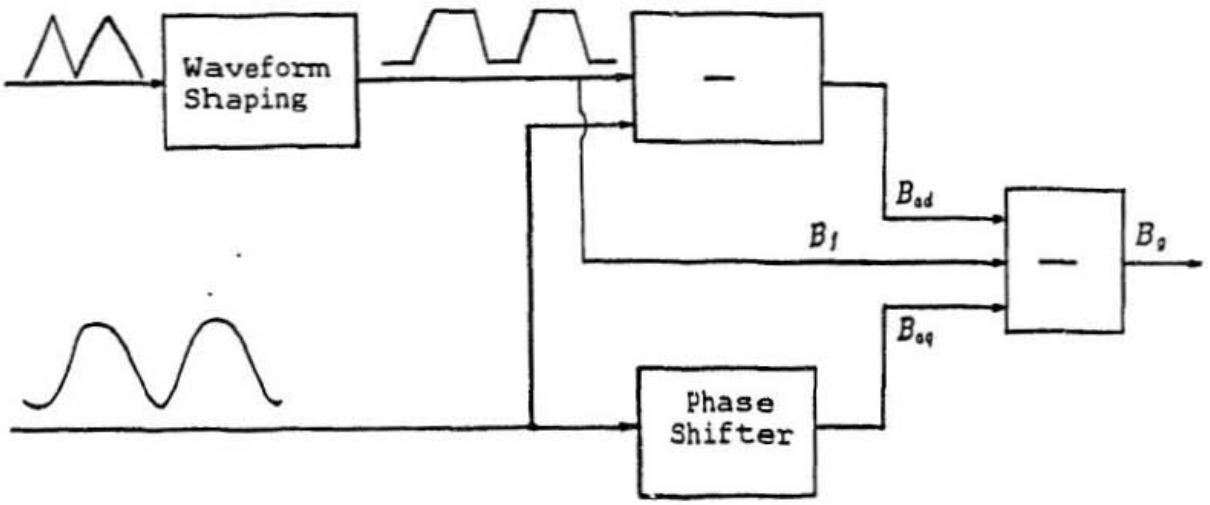

Figure 3.6: Block diagram of analog simulation

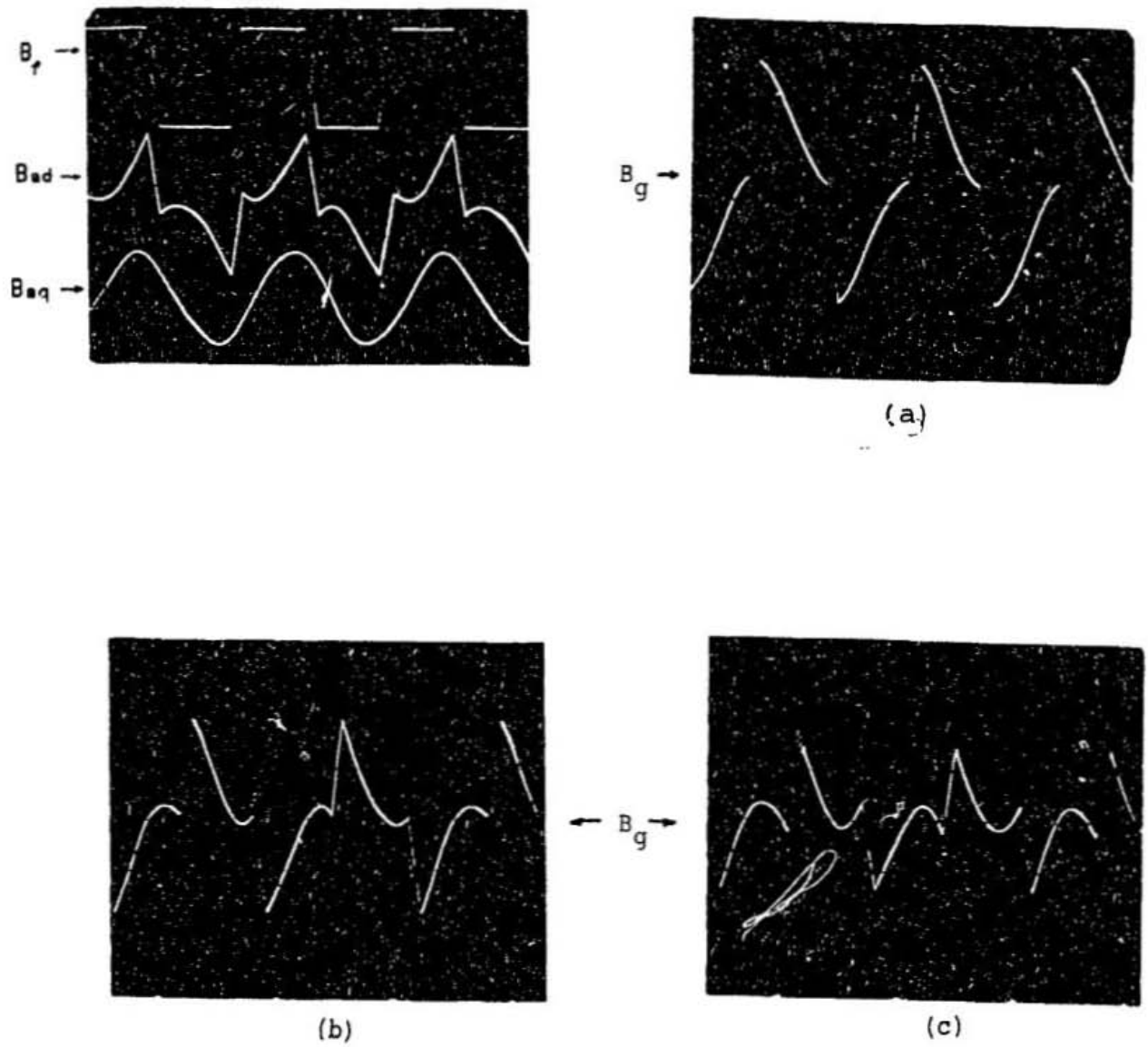

Figure 3.7: Results of air gap field simulation: a) light loading, b) medium loading, c) high loading

- the three air gap components used in the analysis sufficiently describe the actual conditions.
- superposition is valid for general operation and the nonlinear effects are only seen at high loading.

3.4 Digital Measurement of The Motor Torque Angle

In order to calculate the machine parameters from load test it is necessary to measure the torque angle δ, at each load step. The conventional method for measuring this quantity is by use of a stroboscope and graduated disk affixed to the motor frame. The stroboscopic method provides only approximate angular quantities since shaft oscillations and flash irregularities result in a relatively poor measurement accuracy. An alternate digital technique which is both simple and practical for electronic implementation has been developed and is presented in this section.

The torque angle of the P.M. synchronous motor is defined as a angular displacement between the flux components generated by the magnet and applied voltage. Therefore, the torque angle measurement requires the air gap flux waveform as an input and relies upon the fact that the flux component due to the magnet is trapezoidal in shape and that the applied voltage component is sinusoidal. A simulation by use of an analog circuit is carried out to investigate the relationship and is described in Fig.3.9 where B_g is the signal derived from the analog simulation output, see Fig.3.6. The simulation is performed by adjusting the amplitude of the trapezoidal component, E_i and the phase θ_{ph}. Two statements can be drawn from simulation results which is shown in Fig.3.10 and Table 3.1, as follows.

- point P moves directly as the phase θ_{ph} changes:

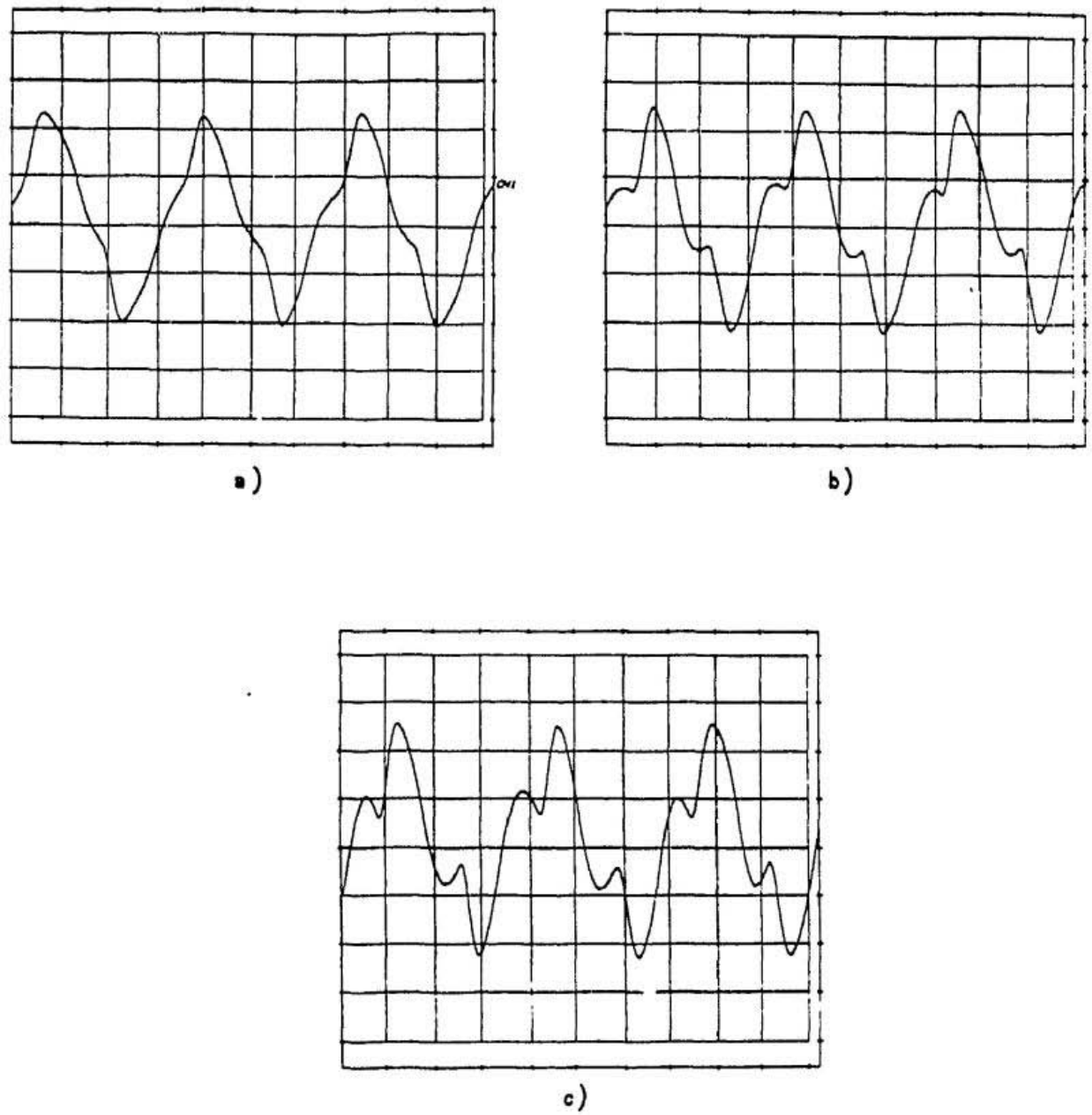

Figure 3.8: Flux waveform distribution obtained from search coil: a) light loading, b) medium loading, c) high loading

- amplitude H varies directly as the amplitude of the trapezoidal component is varied.

The former is useful to measure the torque angle which is given below and the later is helpful to analyze variation of the generated voltage which will be given in the next chapter. The block diagram of the measurement is shown in Fig.3.11 and the circuit is shown in Appendix II. The circuit consists of a flip-flop and a phase detector as well several schmitt triggers and phase shifters. Input of this flip-flop comes from the trapezoidal component in the air gap measured by search coil and the sinusoidal component measured by a voltage transformer. A clipper is used in this measurement circuit to shape the waveform and a voltage follower is used to buffer the output. The schmitt trigger converts a sinusoidal waveform into a rectangular one. At the beginning of the measurement the phase shifter is used to adjust the initial phase angle to zero. As the motor is loaded, the flip-flop produces a signal measured by the phase detector using terminal voltage of the machine as a reference signal. This angular displacement between output of the flip-flop and the reference is a reflection of the motor torque angle. Fig.3.12 presents a comparative results between measured phase θ_{ph} and the torque angle δ measured by the stroboscope. It is clearly shown that they have a good agreement. This technique provides better resolution and is more convenient than the stroboscope method. Furthermore, it can be applied in machine dive systems which require a fast-response digital measurement of the torque angle.

The test methods for determining machine parameters will be given in the next two chapters.

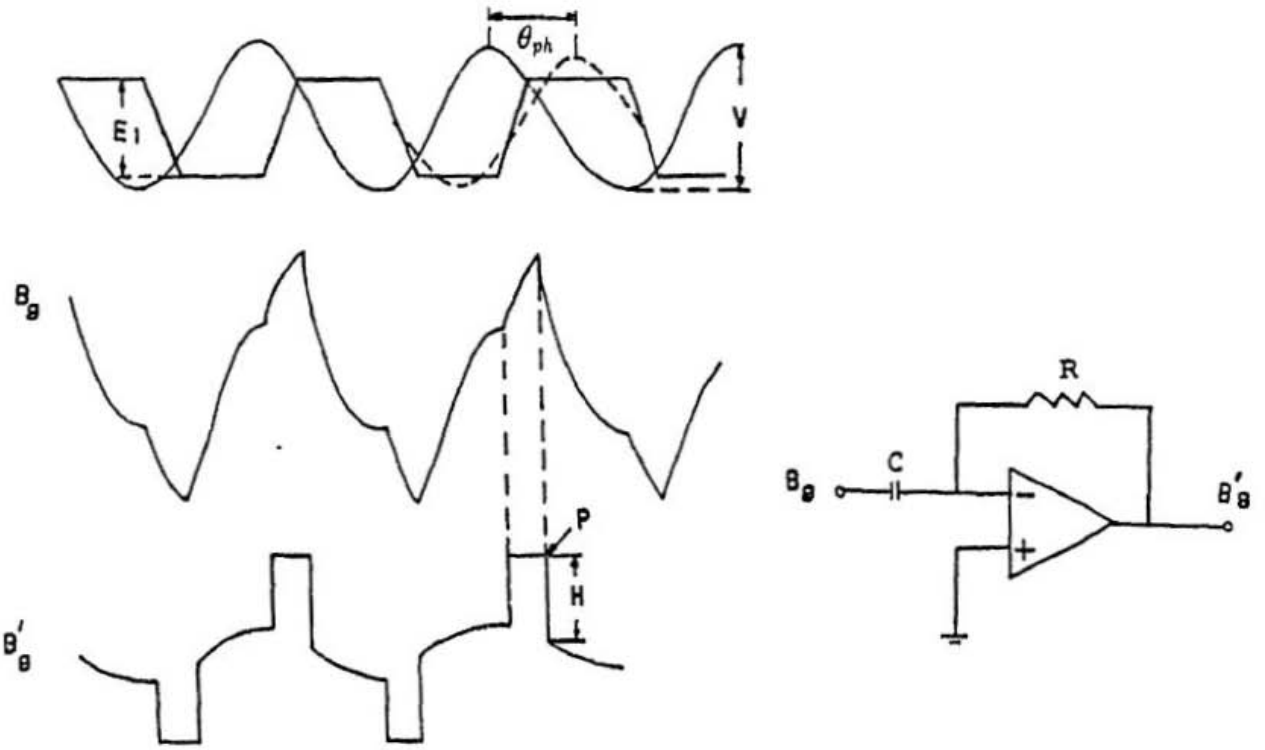

Figure 3.9: Simulation circuit

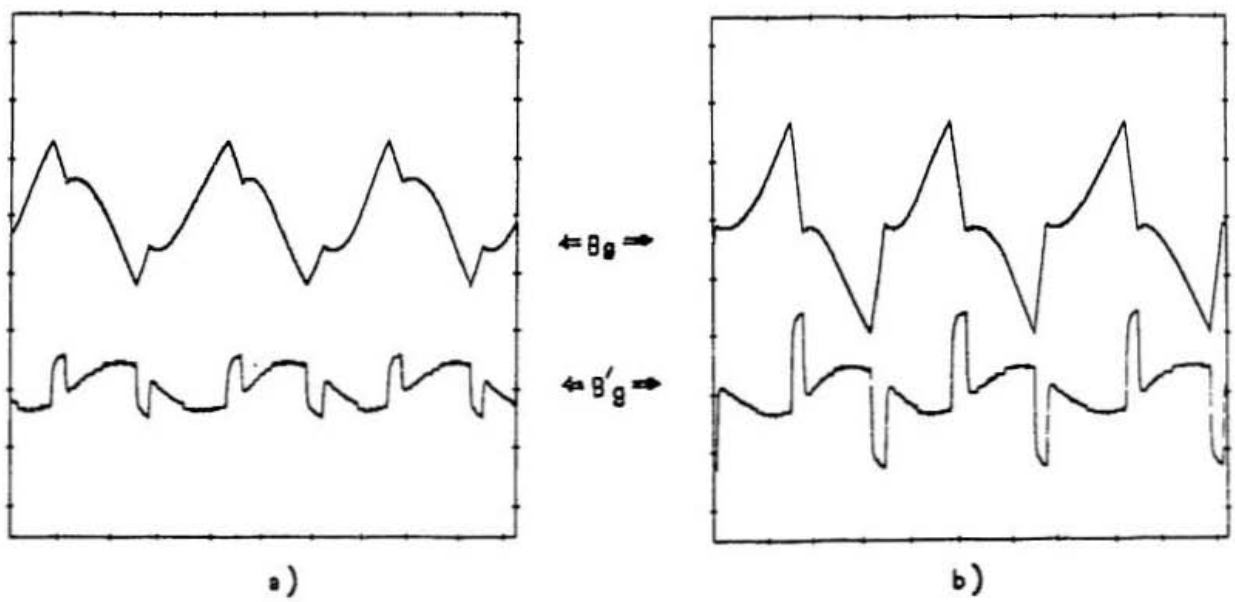

Figure 3.10: Results of simulation : comparison of different amplitude of trapezoidal components - a) smaller amplitude, and b) larger amplitude

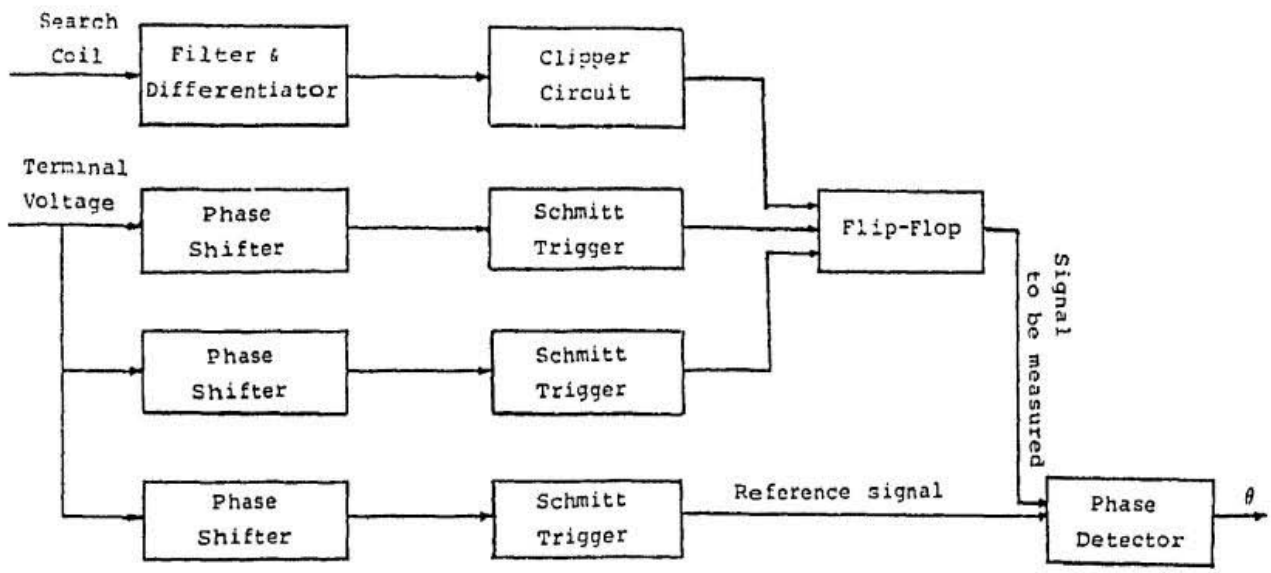

Figure 3.11: Block diagram for torque angle measurement

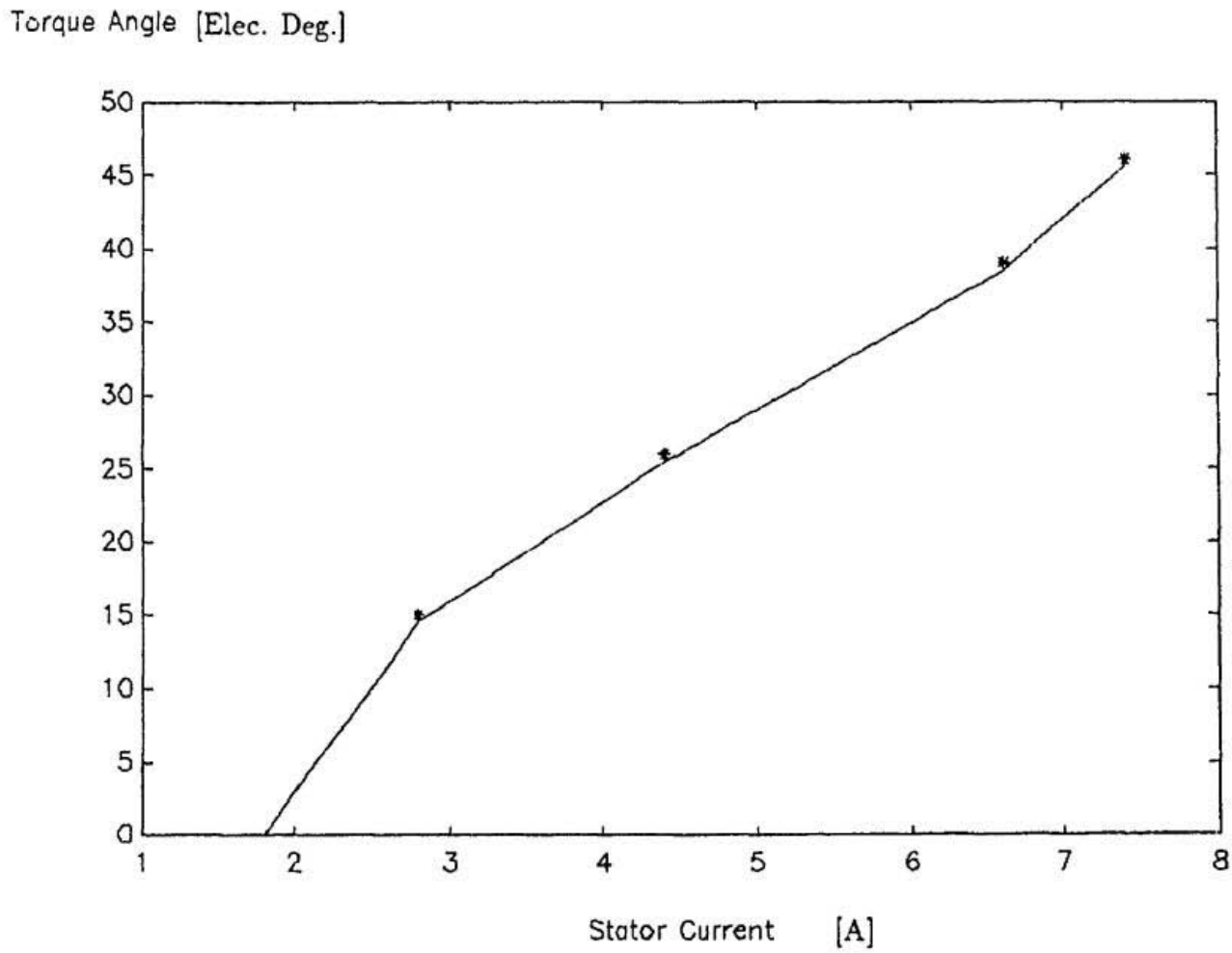

Figure 3.12: Results of the torque angle measurement: line–θ_{ph}, symbol–δ

Table 3.1: Results of analog simulation

E (V)	H (V)	E/H
2.4	1.8	1.33
3.0	2.4	1.25
4.0	3.0	1.33
5.0	3.8	1.32
6.0	4.5	1.33
7.0	5.0	1.40
8.0	6.0	1.33

$E/H_{average} = 1.327$
In this test, $V = 8V$

Chapter 4

DETERMINATION OF P.M. SYNCHRONOUS MOTOR PARAMETERS - PART ONE

4.1 Introduction

Three P.M. synchronous motor parameters were described in the first two chapters and it was shown that the parameters of the machine can be determined by use of computational methods or test methods of which the former is primarily aimed at design work. The work presented here is concerned with the actual measurement. Therefore, a number of different test methods are developed to determine the machine parameters. The machine used in this study is a 3-phase,4-pole, 60 Hz, Y-connected permanent magnet synchronous motor. Its rated speed, voltage and current are 1800 rpm, 208V and 3.0A respectively. In this chapter, the modified conventional tests and search coil test are presented. The main objective of this chapter is to determine the variation of generated voltage under loading which will be used to compute d-axis and q-axis reactances of the machine.

4.2 Modified Conventional Test

Since the special characteristic features of the P.M. synchronous motor are different from the conventional synchronous motor, this results in some difficulties in using conventional test procedures on the P.M. motor. Therefore, the tests including open-circuit and short-circuit tests have to be modified. These tests will be referred to as the "modified conventional test" and are carried out as follows.

4.2.1 Open-Circuit and Short-Circuit Tests

The tests performed on the P.M. synchronous motor are similar to those normally performed on a conventional wound rotor synchronous motor, with the exception that the field excitation cannot be varied. Both open- and short-circuit characteristics are measured while the machine is operating as a generator driven at rated speed. During the open-circuit test, the flux in the the air gap is produced solely by the magnets which induce a voltage in the stator winding called the open-circuit voltage E_0. The short circuit current I_{sc} is used to determine the motor's saturated d-axis reactance X_d, which is approximated by the ratio E_0/I_{sc}. Voltage waveforms measured from the air gap of the machine under both the open- and short-circuit conditions are presented in Fig.4.1 and Fig.4.2 which are recorded by using sensing coils as machine is driven at rated speed and also consistent with that of the air gap field described in preceding chapter. It is clearly shown that the short-circuit current contains significant harmonic component in which the third harmonic is dominate. Therefore, the influence of the third harmonic must be considered when calculating reactance parameters of the machine by use of open-circuit and short-circuit tests. The test data is listed in Table 4.1.

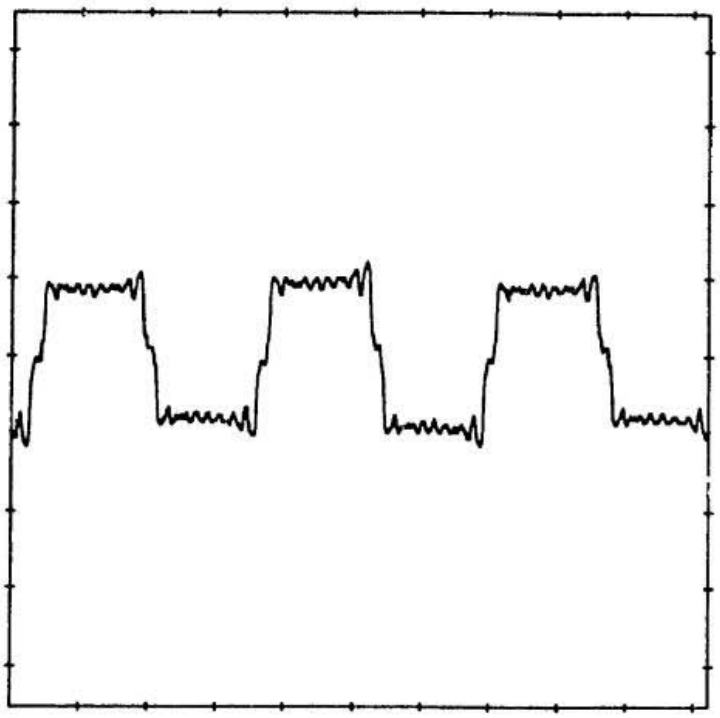

Figure 4.1: Air gap voltage waveform at open-circuit test

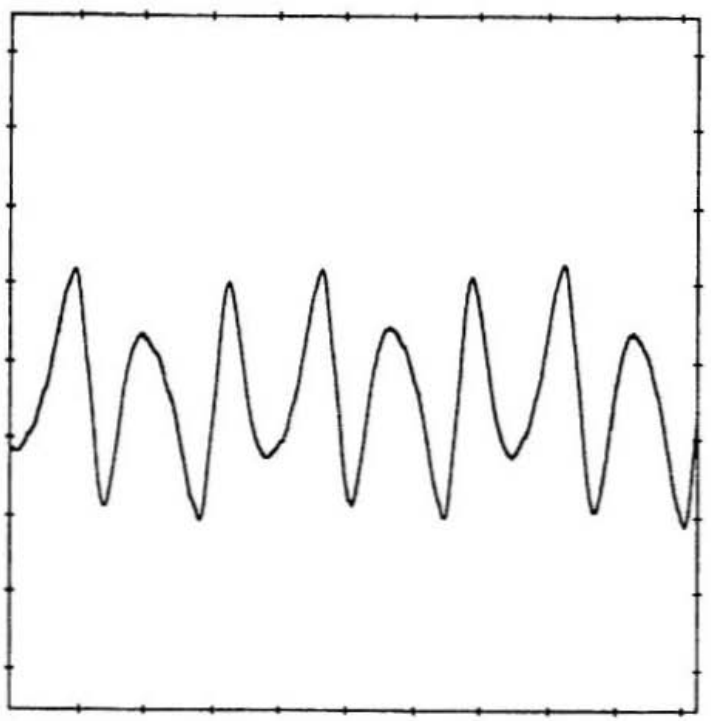

Figure 4.2: Filtered air gap voltage waveform at short-circuit test

4.2.2 No-Load Test

This test is performed on the P.M. synchronous motor while it is running synchronously with no attached load. Table 4.2 shows the test data for the no load current I_{nl} and applied voltage V. Because of the characteristics of P.M. motor, the total torque of the motor can be negative between $\delta = 0$ and $\delta = \delta_0$ at normal supply voltage. Since $\delta = 0$ is generally an unstable point (with $0 > dT/d\delta$), the no-load operation of the motor is at initial torque angle δ_0 which is greater than zero. In order to determine the performance of the motor, the initial torque angle must be considered which can be obtained by use of no-load test. In Eq.(2.5), T_1 is proportional to V and T_2 to V^2, therefore a reduction in the terminal voltage causes a much greater reduction in the reluctance torque than in the excitation torque. This results in a decrease value of δ. It can be observed that the rotor position goes to a minimum angle position which is assumed to be zero torque angle. This angular difference obtained is considered to be approximately δ_0 and will be used later in the load test. For the machine used in this work, $\delta_0 = 22^0$. Up to now, two values of direct-axis reactances have been obtained from these two tests (see Table 4.1 and Table 4.2). These results will be discussed later.

4.2.3 Load Test

The load test provides a means for determining the steady state machine parameters X_d, X_q and E_0 which can be used to calculate motor performance characteristics. The test involves loading the P.M. motor by coupling a synchronous machine or a dynamometer as near as possible to the pull-out value. In this test, sufficient data must be taken to define the phasor diagram uniquely, which includes the applied voltage and current, power factor and torque angle δ. The value of the torque angle δ is either observed by using a stroboscope, or measured from search coil by using the digital circuit which has been given in last chapter. The initial value of torque angle

comes from no load test, see section 4.2.2. The power factor can be measured by two- or three-wattmeter methods and other quantities including supply voltage and current are measured by conventional methods (i.e. voltmeters and ammeters). The load test data is recorded in Table 4.3 and the values of reactance calculated from steady-state voltage equation of the machine [32] are shown in Table 4.4.

4.2.4 Discussion of Test Results

The two points of d-axis reactance at unsaturation and saturation conditions have been determined by use of no-load test, open-circuit and short-circuit tests. Two values are shown in Table 4.1 and Table 4.2. However, since the open-circuit and short-circuit test measurements involve the quantities E_0 and I_{sc}, which are measured at different states of saturation, the direct-axis reactance obtained from this measurement must be considered as approximate value. While measurement of X_d by no-load test is a good approximation at light current level because saturation effects are minimum. The results obtained from the load test are consistent with other published results where the generated voltage is assumed constant at a level of open-circuit value. Note that there is a load range where the value of X_d becomes negative. It means that the machine is behaving as though the d-axis armature reactance were capacitive with constant E_0 behind it. Negative values of X_d are entirely consequent upon the assumption of constant E_0. However, the generated voltage is dependant on the saturation of the steel leakage bridges and thus is a load dependent variable. Therefore, the reactance parameters calculated based on assumption of the constant generated voltage at loading and shown in Table 4.4 may result in some error when used to predict performance. It is necessary now to determine how the air gap voltage changes and what factors influence this variation.

Table 4.1: Open-circuit and short-circuit test results

E_0 (V)	I_{sc} (A)	X_d^1 (Ω)
118.0	4.5	15.1

Table 4.2: No-load test results

E_0 (V)	V (V)	I_{nl} (A)	X_d^2 (Ω)
118.0	197.0	1.8	25.3

where

$X_d^1 = \frac{E_0}{\sqrt{3} I_{sc}}$: saturated value
$X_d^2 = \frac{V - E_0}{\sqrt{3} I_{nl}}$: unsaturated value
and $\delta_0 = 22^0$

Table 4.3: Load test

V (V)	P (W)	I_a (A)	δ (Elec.Deg.)
202	350	1.80	3.0
202	500	2.10	6.0
202	600	2.40	8.0
202	710	2.70	12.0
202	820	3.00	14.4
202	890	3.25	16.0
202	1000	3.50	18.0
202	1160	4.05	23.0
202	1320	4.60	26.0
202	1400	4.85	28.0
202	1525	5.35	34.0
202	1650	5.85	36.0
202	1700	6.15	38.0
202	1840	7.00	42.0
202	1900	8.10	52.0

Table 4.4: D-axis and Q-axis reactances

I_a (A)	I_d (A)	I_q (A)	X_d (Ω)	X_q (Ω)
1.8	1.013	1.488	37.040	30.633
2.1	0.688	1.984	45.692	28.243
2.4	0.597	2.325	48.291	25.565
2.7	0.342	2.678	69.742	24.589
3.0	0.117	2.998	175.104	23.166
3.25	0.028	3.25	642.145	22.110
3.5	-0.290	3.448	-51.732	21.338
4.1	-0.700	3.989	-10.217	20.345
4.6	-1.043	4.480	-1.746	18.910
4.8	-1.303	4.672	1.235	18.603
5.3	-1.879	5.009	6.383	18.600
5.8	-2.165	5.435	7.483	17.454
6.2	-2.323	5.695	8.686	16.974
7.0	-2.701	6.458	10.658	15.450
8.1	3.563	7.274	13.834	14.496

$$X_d = \frac{V\cos\delta - E_0}{I_a \sin(\phi-\delta)} - \frac{R_1 I_a \cos(\phi-\delta)}{I_a \sin(\phi-\delta)}$$
$$X_q = \frac{V\sin\delta}{I_a \cos(\phi-\delta)} + \frac{R_1 I_a \sin(\phi-\delta)}{I_a \cos(\phi-\delta)}$$

4.3 Search Coil Simulation

The idea of this test comes from the analog simulation of the air gap fields, see section 3.3 and section 3.4, and its results, see Fig.3.9 and Fig.3.10. The simulation has shown that there is a linear relationship between the discontinuity amplitude denoted by H, and the amplitude of the trapezoidal component denoted by E_i. This gives a means for determining the variation of the generated voltage. The test procedure is as follows. While the P.M. machine is operating as a generator driven at rated speed, the air gap flux waveform is measured by use of the search coils and low-pass filtered to remove tooth ripple harmonics. The output of the filter is differentiated and result is recorded in the Fig.4.3. The P.M. motor is loaded by coupling a synchronous machine, while the air gap flux of the P.M. motor is measured from search coils and is taken as a input of the test circuit. With different loading, the stator current I_a and discontinuity amplitude H are recorded as shown in Table 4.5. Fig.4.4 shows both results of open circuit and load test.

The generated voltage can now be determined from the search coil test results. The calculation assumes that $E/E_0 = H/H_0$ which is verified from the analog simulation of the air gap filed. Results which show the variation tendency of the generated voltage with increasing load are presented in Table 4.6 and Fig.4.5. In Fig.4.5, however, only the two values shown at point A and point B can be validated. The reason for this is that E_i obtained from search coil test includes two components given by the field equations (see last chapter). One is due to the field strength of the magnet sections B_f and another due to armature reaction in direct-axis B'_{ad}, which are repeated for convenience below:

$$B_f = \frac{B_r (A_m / A_g)}{1 + \beta K_l} \tag{4.1}$$

$$B'_{ad} = \frac{2/\pi}{1 + \beta K_l} * \frac{0.4\mu_0^2 F_{dm}}{g} \tag{4.2}$$

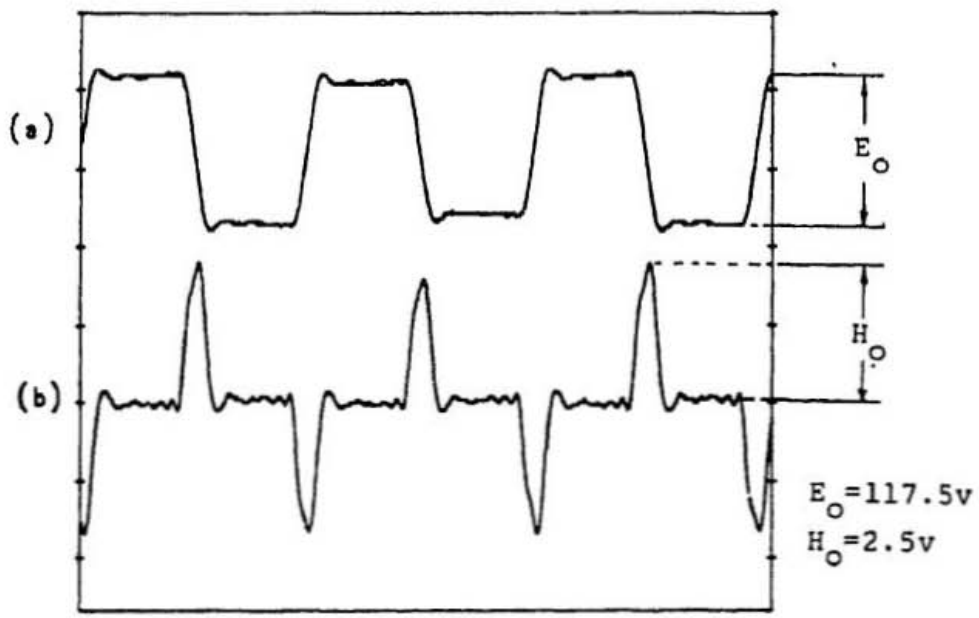

Figure 4.3: Result of simulation: (a) input of the differentiator, (b) output of the differentiator

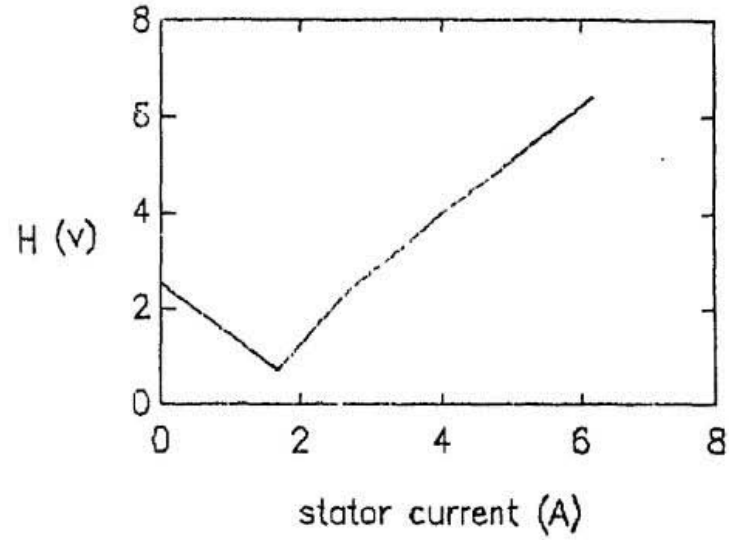

Figure 4.4: Search coil simulation - open circuit test and load test

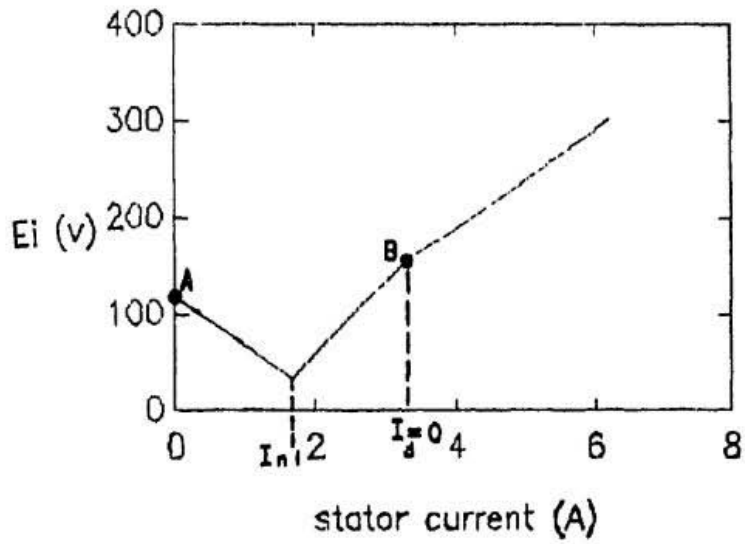

Figure 4.5: Determination of generated voltage

where

$$F_{dm} = \frac{0.9\, m\, I_d\, N\, K_w}{P} \tag{4.3}$$

But, no armature reaction occurs at either point A which is the open-circuit value or point B at which I_d equals zero (I_d=$I_a\ sin(\phi - \delta) = 0$ when power factor ϕ equals torque angle δ). Since these two points contain no direct-axis armature reaction, they can be used to calibrate the test procedure. The value of generated voltage at point B can also be obtained from the phasor diagram associated with the moment of zero d-axis armature reaction, see Fig.4.6. At this moment, ϕ=δ=38^0, $E_i = V\ cos\phi$ = 159.2V (V = 202V). This value is included in Table 4.6 for comparison. It is clear that the values obtained from search coil simulation and from phasor diagram have a good agreement. The value of saturated E_i evaluated from this point is more close to that at short circuit than E_0 at open circuit. Consequently, it is used to recomputed saturated value of X_d as: $X_d = E_i/\sqrt{3}{*}I_{sc}$ = 20.5 (Ω). This value will be used to compare with that from other methods later.

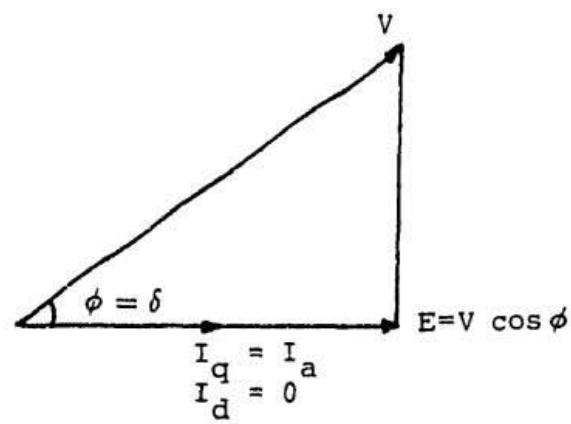

Figure 4.6: Phasor diagram ($\phi = \delta$)

Up to now, two values of generated voltage at different load conditions have been

evaluated. One is the open circuit value and the another corresponds to a condition of zero d-axis current. The two conditions have different values corresponding to different loads. The reason for the variation of generated voltage under load is given below. Upon examination of the phasor diagram and the flux linkage paths of the rotor under different load conditions, see Fig.4.7 - Fig.4.8, it is observed that the applied voltage results in a magnetizing current I_d at light load, which will increase saturation of the main flux paths and reduce saturation of the rotor steel bridges. A positive I_d, therefore, will result in a decrease of generated voltage E_i. On the other hand, at heavy load, the armature reaction becomes magnetizing with respect to the magnets and demagnetizing with respect to the steel bridges which results in an increase of generated voltage E_i. In Fig.4.8, Φ_d is referred to the flux due to the armature reaction, Φ_m to the flux due to the magnets and Φ_l is the leakage flux of the steel bridges. Influence of the armature reaction will be studied in the next section.

Table 4.5: Search coil simulation - load test

I_a (A)	H (V)
1.7	0.7
2.2	1.6
2.7	2.4
3.2	3.4
4.2	4.0
4.8	4.8
5.5	5.6
6.2	6.4

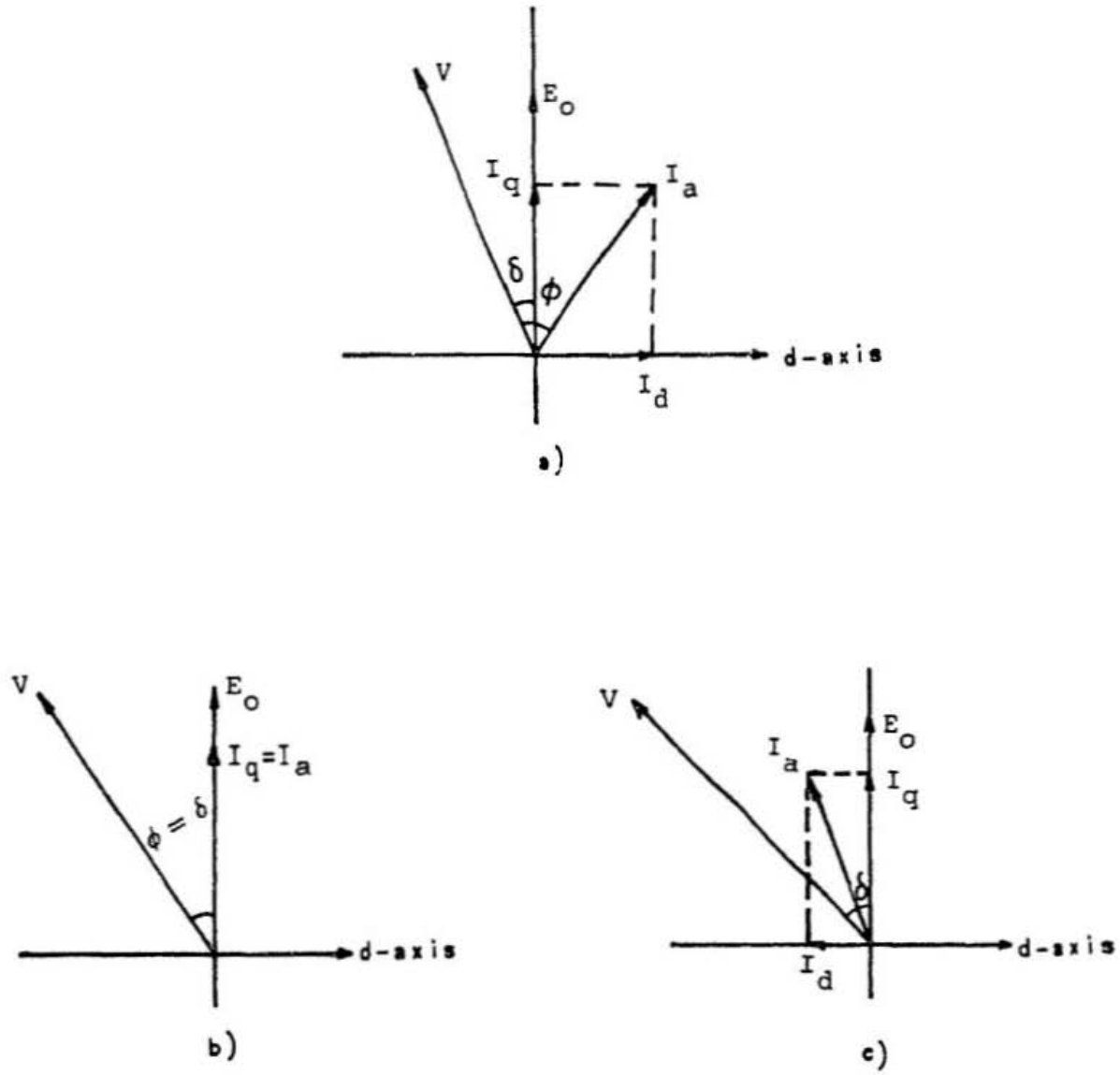

Figure 4.7: Stator current at different load condition a) light loading: magnetizing I_d, b) δ=ϕ: I_d=0 and I_q=I_a, c) heavy loading: demagnetizing I_d

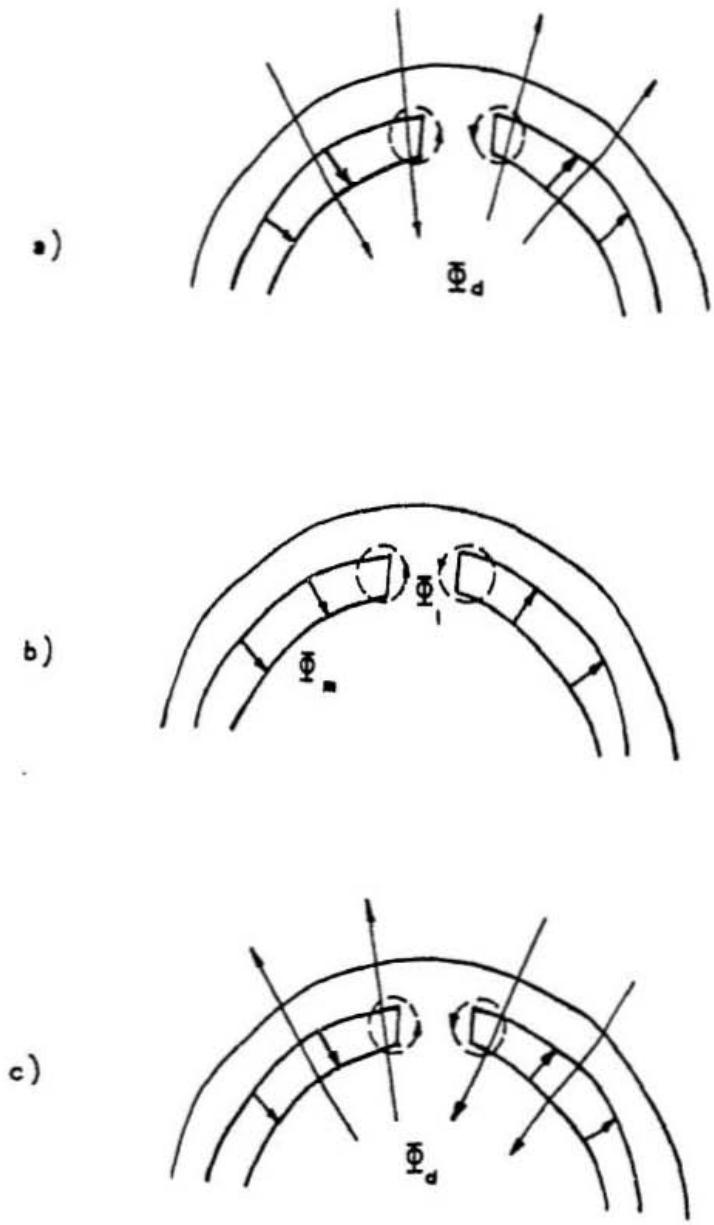

Figure 4.8: Armature reaction a) magnetizing I_d, b) I_d=0, c) demagnetizing I_d

Table 4.6: Determination of generated voltage from search coil simulation

I_a (A)	H (V)	E_1 (V)	$E = V\cos\phi$ (V)
1.7	0.7	32.9	
2.2	1.6	75.2	
2.7	2.4	112.8	
3.2	3.4	159.8	159.2
4.2	4.0	188.0	
4.8	4.8	225.6	
5.5	5.6	263.2	
6.2	6.4	300.8	

where

$$E = E_0 \frac{H}{H_0}$$
$$E_0 = 117.5V$$
$$H_0 = 2.5V$$

4.4 Influence of Armature Reaction on Generated Voltage

The influence of armature reaction on the generated voltage under loading is investigated on the specific rotor structure which was designed by T.A.Little [2]. Recalling the three flux density field equations as follows:

$$B_f = \frac{B_r (A_m / A_g)}{1 + \beta K_l} \tag{4.4}$$

$$B_{ad} = \frac{0.4\mu_0 \pi F_{dm}}{g} [cos \frac{P}{2}\theta - \frac{2\mu_0/\pi}{1 + \beta K_l}] \tag{4.5}$$

$$B_{aq} = \frac{0.4\mu_0 \pi F_{qm}}{g} sin \frac{P}{2}\theta \tag{4.6}$$

The total air gap field is given as:

$$B_g = B_f + B_{ad} + B_{aq} \tag{4.7}$$

The above equation shows that there are two components affected by the saturation factor, one being B_f caused by magnet sections, the other being $B'_{ad}=\frac{0.8\mu_0^2 F_{dm}/g}{1+\beta K_l}$ caused by armature reaction. Both of these components combine to produce the voltage E_t that is measured by the search coil and has been recorded in Table 4.6. The influence of the leakage factor $K = \frac{1}{1+\beta K_l}$ in B_{ad} will be investigated as follows based on the rotor structure with dimensions, parameters and flux paths are given in Appendix III and taken from reference [2]. Assume that the leakage factor is,

$$K = \frac{1}{1 + \beta K_l} \tag{4.8}$$

where

$$\beta = \frac{2R_g}{R_m}$$

$$K_l = 1 + \frac{R_m}{R_l}$$

Calculating reluctance values in various flux paths, gives:

$$\begin{aligned} R_g &= \frac{g}{\mu A_g} \\ &= \frac{g}{\mu l_s \pi D} \\ &= \frac{0.0033 \times 2}{1.0 \times 7.62 \times 3.14 \times 6.85} \\ &= 0.0004025\,42\ amp-turns/weber \end{aligned} \tag{4.9}$$

$$\begin{aligned} R_m &= \frac{1}{\frac{1}{R_{m1}} + \frac{1}{R_{m2}}} \\ &= \frac{1}{74.1 + 27.5} \\ &= 0.009\ amp-turns/weber \end{aligned} \tag{4.10}$$

where

$$\begin{aligned} R_{m1} &= \frac{L_1}{\mu_1' 2 l_s h_1} \\ &= \frac{0.559}{1.014 \times 2 \times 7.62 \times 0.996} \\ &= 0.036318\ amp-turns/weber \end{aligned} \tag{4.11}$$

$$\begin{aligned} R_{m2} &= \frac{L_2}{\mu_2' 2 l_s h_2} \\ &= \frac{0.559}{1.014 \times 2 \times 7.62 \times 2.68} \\ &= 0.013492\ amp-turns/weber \end{aligned} \tag{4.12}$$

Thus,

$$\begin{aligned} \beta &= 2R_g / R_m \\ &= 0.09 \end{aligned} \tag{4.13}$$

$$\begin{aligned} K_l &= 1 + \frac{R_m}{R_l} \\ &= 1 + \frac{0.009}{R_l} \end{aligned} \tag{4.14}$$

R_l is reluctance of leakage path and a key parameter which affects B'_{nd}. Since all the leakage paths for the given rotor configuration are in parallel (Appendix *III*), R_l

can be written as:

$$\begin{aligned} R_l &= \frac{1}{\frac{1}{R_{l1}} + \frac{1}{R_{l2}} + \frac{1}{R_{l3}} + \frac{1}{R_{l4}}} \\ &= \frac{1}{\frac{\mu}{12.7} + \frac{\mu}{4.4} + \frac{\mu}{5.9} + \frac{\mu}{3.7}} \\ &= \frac{1.34}{\mu}\ amp-turns/weber \end{aligned} \tag{4.15}$$

where

$$R_{l1} = \frac{L_1}{2\,B_{L1}\,\mu_1\,T_1} = \frac{12.7}{\mu}\ amp-turns/weber \tag{4.16}$$

$$R_{l2} = \frac{L_2}{2\,B_{L2}\,\mu_2\,T_2} = \frac{4.4}{\mu}\ amp-turns/weber \tag{4.17}$$

$$R_{l3} = \frac{L_3}{2\,L_3\,\mu_3\,T_3} = \frac{5.9}{\mu}\ amp-turns/weber \tag{4.18}$$

$$R_{l4} = \frac{L_4}{2\,L_4\,\mu_4\,T_4} = \frac{3.7}{\mu}\ amp-turns/weber \tag{4.19}$$

To simplify the problem currently studied, the permeability of all the leakage paths are assumed to be the same, although they are not equal in practice. The permeability of the steel bridges μ is a function of the field strength H. This varies with loading condition and shifts the operating point along the BH characteristic shown in Fig.4.9. Investigation is based on the variation of field strength at different loading conditions. The total flux density on the magnet face(one of the magnet sections) is described by $B_m = B_r - \mu' H + \mu' H'$. The armature reaction component $\mu' H'$ can be magnetizing or demagnetizing depending on the sign of F_{dm} which is determined by the sign of I_d given in Eq.4.3. At the open circuit point where I_d equals zero, $B_m = B_r - \mu' H$. When loading the machine, the operating point will move up to where the power factor ϕ

equals torque angle δ, and after that I_d will change sign and be demagnetizing, thus the operating point will move down. Therefore, the permeability μ is higher at open circuit condition and lower under load condition. The leakage factor is:

$$\begin{aligned} K &= \frac{1}{1+\beta K_l} \\ &= \frac{1}{1+0.09\left(1+\frac{R_m}{R_l}\right)} \\ &= \frac{1}{1.09+0.0006\mu} \end{aligned} \tag{4.20}$$

Assuming μ=5000 at unsaturation and μ=10 at saturation. Thus,

$$\begin{aligned} K &= 4.09 \qquad \textit{at saturation} \\ K &= 0.115 \qquad \textit{at unsaturation} \end{aligned} \tag{4.21}$$

It is clear that the leakage factor consists of both magnet and armature reaction components and has significantly different values at different load conditions. The contribution of the armature reaction component to the generated voltage is difficult to calculate because of the nonlinearity of the magnetic materials. The determination of B'_{ad} will not be considered at this moment. From consideration of leakage factor K, a general statement can be drawn as follows: At light loading, B'_{ad} has a negative sign which makes the measured voltage decrease below the actual generated voltage. As the load is increased, B'_{ad} will change sign, causing in the measured voltage to increase above the actual generated voltage. Fig.4.10 shows the effects of removing the armature reaction component to obtain the actual magnet generated voltage E_0. In order to simply calculations two values of E_0 will be chosen to approximate the variation of the generated voltage (see Fig.4.10). Using these two values the reactance parameters can now be computed as shown in Table 4.1 and Fig.4.11. It is clearly shown that in Fig.4.11 there is an intermediate range of loads where d-axis reactance becomes difficult to determine. This is in the range where the armature reaction

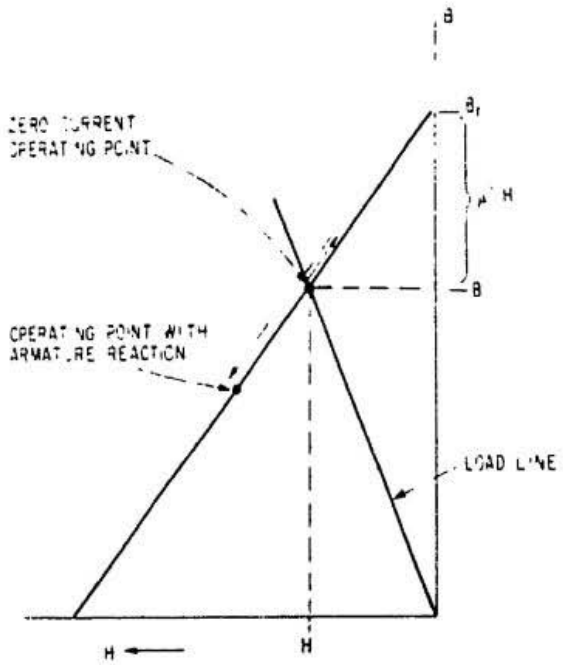

Figure 4.9: Operating point at different load

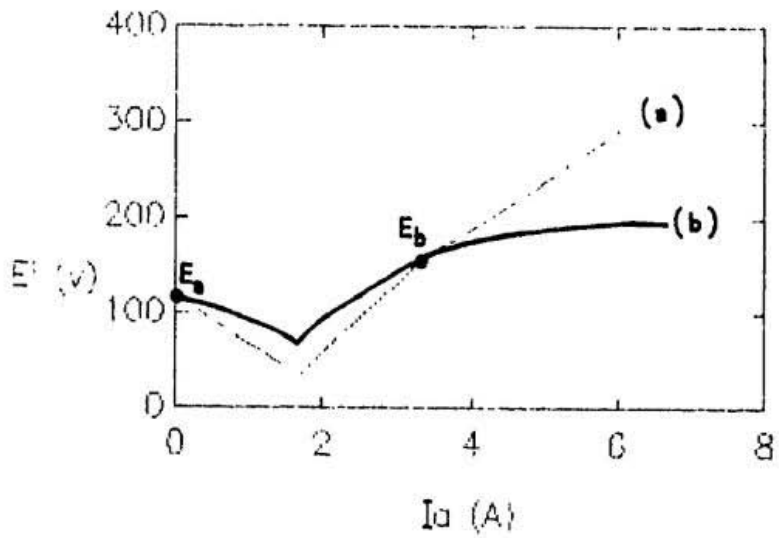

Figure 4.10: Variation of the generated voltage(a):measured E_t- including the armature reaction component (b):estimated actual E_0- separated from the armature reaction and considered leakage factor

in the d-axis is changing from a condition of "magnetizing" the magnets to one of demagnetizing them. The value of X_d derived from the steady-state voltage equation of the machine is extremely sensitive to the accuracy of the experimental measurements. The negative values of X_d do not appear in any range of loads as compared with Table 4.4 in which the d-axis reactance is determined using the assumption of constant E_0. This is consistent with the statement that negative values for X_d are entirely consequent upon the assumption of constant E_0 and do not imply anything impossible about the machine.

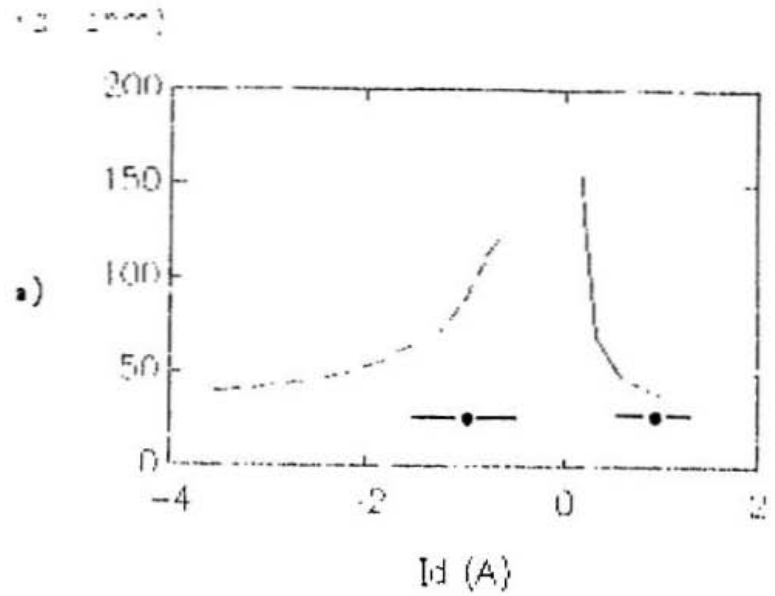

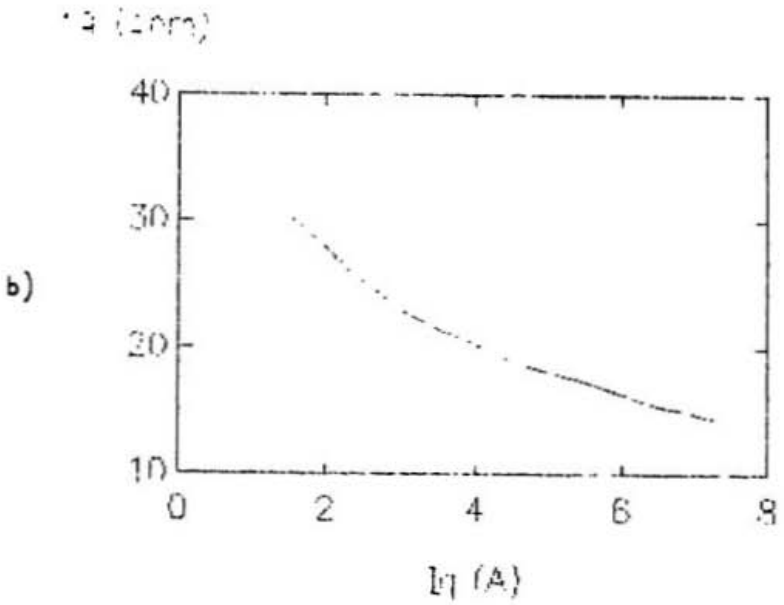

Figure 4.11: Reactance parameters a) d-axis and b) q-axis

•– modified conventional tests

Table 4.7: D-axis and Q-axis reactances

I_a (A)	I_d (A)	I_q (A)	X_d (Ω)	X_q (Ω)
1.80	1.013	1.488	37.040	30.633
2.10	0.688	1.984	45.692	28.243
2.40	0.597	2.325	48.291	25.565
2.70	0.342	2.678	69.742	24.589
3.00	0.117	2.998	175.104	23.160
3.50	-0.29	3.488	263.097	21.338
4.05	-0.7	3.989	120.069	20.345
4.60	-1.043	4.48	85.692	18.910
4.85	-1.303	4.672	71.172	18.603
5.35	-1.879	5.009	54.909	18.600
5.85	-2.165	5.435	49.592	17.454
6.15	-2.323	5.695	47.934	16.974
7.00	-2.701	6.458	44.403	15.450
8.10	-3.563	7.247	39.416	14.496

Chapter 5

DETERMINATION OF P.M. SYNCHRONOUS MOTOR PARAMETERS - PART TWO

5.1 Introduction

The modified conventional test and the search coil simulation presented in the last chapter were used to locate two specific values of d-axis reactance and to show the variation of generated voltage under load conditions. In this chapter, additional test methods, which employ the flux linkage test and the search coil test to determine P.M. synchronous motor parameters are presented. The tests are performed on the same motor used in the tests described in the last chapter.

5.2 Flux Linkage Test

The flux linkage test, which is based on the theory of operation introduced by C.V.Jones [29] can be applied to the measurement of the inductance of the P.M. motor. This was first proposed by Miller [19] and later used by Little [2]. The method

is used for measuring static inductance without being affected by the presence of the magnet flux or by induced current in the starting cage. The measurement circuit shown in Fig.5.1 satisfies these requirements. Strictly speaking, the test measures the flux linkage of the winding rather than the inductance itself. This bridge circuit is composed of two non-inductive resistors (R_3 and R_4) and one variable non-inductive resistor (R_2) used to balance the bridge circuit. Also one dc power supply (V) and one on-off switch (S) are included in this circuit. The R_1 and L represent the self-inductance and resistance of the machine winding. The voltage across the bridge is observed and measured by use of an oscilloscope.

5.2.1 Theory of Operation

When the switch of Fig.5.1 is closed with the rotor and stator aligned along the direct-axis (or quadrature-axis), a constant current I establishes a field in the stator winding. After balancing the bridge (i.e. $V_{ab} = 0$) and then opening the switch the current I through the inductor will fall exponentially to zero. Assuming v_{ab} is the instantaneous voltage across the bridge during this transient period. Thus,

$$v_{R3} = R_3 \frac{v}{R_3 + R_1} \tag{5.1}$$

$$v_{R2} = R_2 [\frac{v}{R_1 + R_2} - \frac{1}{R_1 + R_2} L \frac{di}{dt}] \tag{5.2}$$

and

$$\begin{aligned} v_{ab} &= v_{R3} - v_{R2} \\ &= v [\frac{R_3}{R_3 + R_1} - \frac{R_2}{R_1 + R_2}] - \frac{R_2}{R_1 + R_2} L \frac{di}{dt} \end{aligned} \tag{5.3}$$

Since the bridge is balanced,

$$\frac{R_3}{R_4} = \frac{R_2}{R_1} \tag{5.4}$$

Thus,

$$v_{ab} = (\frac{R_2}{R_1 + R_2}) L \frac{di}{dt} \tag{5.5}$$

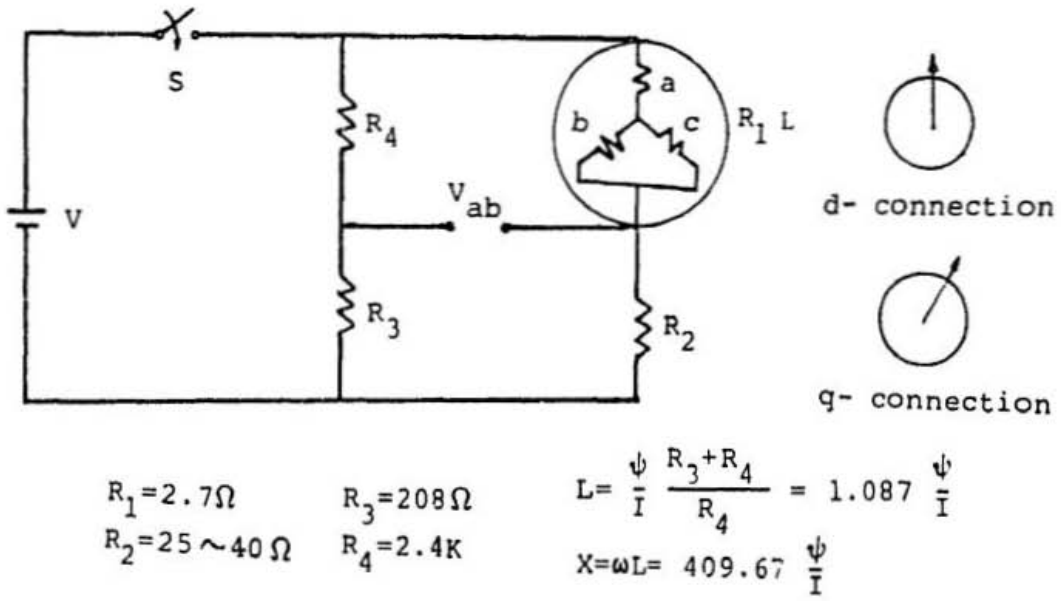

Figure 5.1: Flux linkage test circuit

The flux linkage can be obtained by integrating this transient voltage:

$$\begin{aligned} \psi &= \int_0^\infty v_{ab}\, dt \\ &= \int_I^0 \frac{L R_2}{R_1 + R_2}\, dI \\ &= \frac{R_2}{R_1 + R_2} L I \end{aligned} \tag{5.6}$$

or

$$\begin{aligned} L &= \frac{\psi}{I} \frac{R_1 + R_2}{R_1} \\ &= \frac{\psi}{I} \frac{R_3 + R_4}{R_1} \end{aligned} \tag{5.7}$$

Therefore, integrating the voltage change across the bridge gives an indication of the inductance along the axis of the alignment.

5.2.2 D- and Q - Axes Connection

Once the bridge circuit is connected to the power supply, a dc field is established in the stator winding. For the machine used in this work, the rotor has four poles. Thus, the mechanical angle between d-axis and q-axis is 45 degrees. The d-axis of the rotor will align with the axis of the phase of stator winding automatically when the power supply is connected to the bridge circuit. The q-axis can be found by rotating the rotor through 45 mechanical degrees from the d-axis position. The results of measurement are shown in Tables 5.1-5.2.

5.2.3 Discussion

The test results, including modified conventional tests and flux linkage measurement are shown in Fig.5.2. This figure shows a reasonable correlation for the d-axis reactance. Since this test is a static measurement, it provides a means for separating

generated voltage E_t and d-axis reactance X_d in which the difficulties of measuring X_d is avoided. Therefore, the results from this test is more accurate. Secondly, it presents the values of X_d at entire loads range. However, the thermally induced resistance variation in the bridge components leads to a difficulty in maintaining a balanced condition. This factor prevents this technique from being used for high current values. Therefore, resistances with lower temperature sensitivity are suggested.

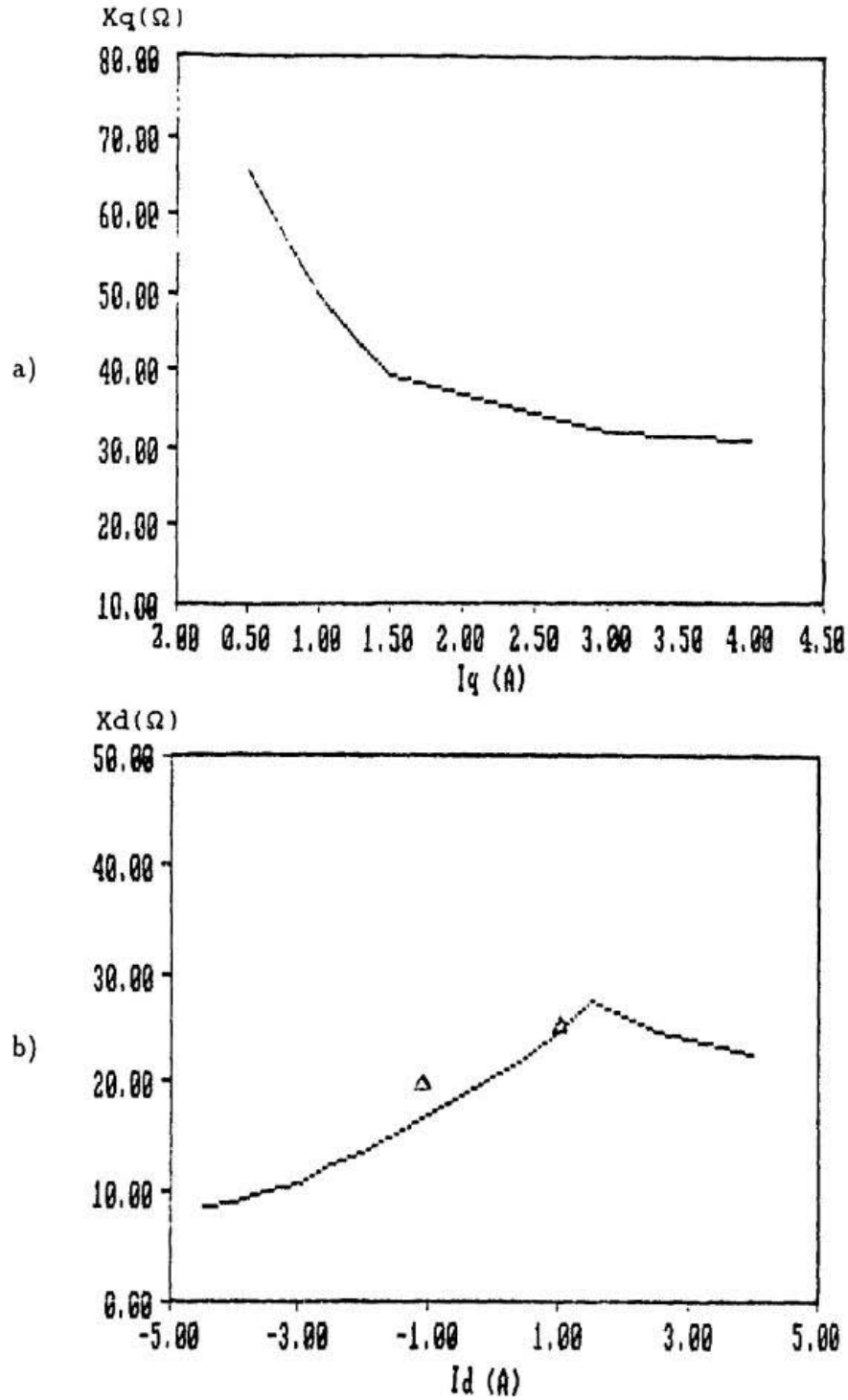

Figure 5.2: Results of flux linkage test: a) q-axis b) d-axis: symbol–modified conventional test results

Table 5.1: Results of flux linkage test: d-axis reactance

I_d (A)	$\int v_{ab}$ (V)	ψ (wb)	X_d (Ω)
-5.0	10.0	0.1	8.2
-4.5	9.5	0.095	8.6
-4.0	9.0	0.09	9.2
-3.5	8.5	0.085	9.95
-3.0	8.0	0.08	10.9
-2.5	7.6	0.076	12.5
-2.0	6.7	0.067	13.7
-1.5	6.0	0.06	16.4
-1.0	4.6	0.046	18.8
-0.5	2.4	0.024	19.7
0.5	2.7	0.027	22.1
1.0	6.0	0.06	24.6
1.5	10.0	0.1	27.3
2.0	13.0	0.13	26.6
2.5	15.0	0.15	24.6
3.0	18.0	0.18	21.6
3.5	20.0	0.2	23.4
4.0	22.0	0.22	22.5

Table 5.2: Results of flux linkage test: q-axis reactance

I_q (A)	$\int v_{ab}$ (V)	ψ (wb)	X_q (Ω)
0.5	8.0	0.08	65.5
1.0	12.0	0.12	19.2
1.5	14.1	0.111	39.3
2.0	20.0	0.2	40.9
2.5	22.0	0.22	36.0
3.0	24.0	0.21	32.0
3.5	29.0	0.29	33.9
4.0	30.0	0.3	30.7

5.3 Search Coil Test

Lipo [33] and Plunkett [34] have presented the use of search coils in AC induction motors for drive application. This method can also be used to measure the air gap flux distribution of the P.M. motor [23]. In this section, d- and q-axis reactance measurement by use of flux sensing coils is described.

5.3.1 Theory of Operation

The test method is based on the two-axis theory in which the time-varying parameters are eliminated. The variables and parameters are expressed in terms of direct- and quadrature-axis quantities [35-36]. The d-q dynamic model of a machine can be expressed in either a stationary or a rotating reference frame. This study uses the stationary reference frame. According to the axes transformation, the phase voltages in terms of d- and q- voltages can be written in matrix form as:

$$\begin{bmatrix} v_a \\ v_b \\ v_c \end{bmatrix} = \begin{bmatrix} cos\theta & sin\theta & 1 \\ cos(\theta - 120^0) & sin(\theta - 120^0) & 1 \\ cos(\theta + 120^0) & sin(\theta + 120^0) & 1 \end{bmatrix} \begin{bmatrix} v_q \\ v_d \\ v_0 \end{bmatrix} \tag{5.8}$$

The other quantities, such as current and flux can be transformed in a similar manner. The corresponding inverse relation is given by:

$$\begin{bmatrix} v_q \\ v_d \\ v_0 \end{bmatrix} = \frac{2}{3} \begin{bmatrix} cos\theta & cos(\theta - 120^0) & cos(\theta + 120^0) \\ sin\theta & sin(\theta - 120^0) & sin(\theta + 120^0) \\ 0.5 & 0.5 & 0.5 \end{bmatrix} \begin{bmatrix} v_a \\ v_b \\ v_c \end{bmatrix} \tag{5.9}$$

where v_0 is the zero-sequence component.

For balanced three-phase condition, the zero-sequence component does not exit. The angle θ between the two sets of axes is arbitrary . It is convenient to set $\theta = 0$, so that the q-axis is coincident with the a-axis. Also ignoring the zero-sequence

component, the transformation relations can be simplified as:

$$\begin{aligned} v_q &= \frac{2}{3}[\, v_a cos\theta + v_b cos(\theta - 120^0) + v_c cos(\theta + 120^0)\,] \\ &= \frac{2}{3}[\, v_a + \frac{1}{2}v_a] \\ &= v_a \end{aligned} \tag{5.10}$$

$$\begin{aligned} v_d &= \frac{2}{3}[\, v_a sin\theta + v_b sin(\theta - 120^0) + v_c sin(\theta + 120^0)\,] \\ &= \frac{2}{3}[\frac{\sqrt{3}}{2}(v_c - v_b)] \\ &= \frac{1}{\sqrt{3}}(v_c - v_b) \end{aligned} \tag{5.11}$$

Therefore, the implementation of d- and q- voltages can be realized by using the three-phase voltage v_a, v_b and v_c. The block diagram of the measurement realization is shown in Fig.5.3. The three phase voltages v_a, v_b and v_c are air gap voltages. Y_s represents an integrator through which the voltage quantity is transformed into the flux quantity. D-axis quantity can be evaluated by subtracting the quantities of b phase from c phase and multiplying a coefficient. These can be implemented from a subtractive and a proportional circuits, both of which are op-amplifier base circuits.

5.3.2 Installation of Flux Coils

The motor used in this study has 36 stator teeth and the flux coils are arranged concentrically around stator tooth as shown in Fig.5.4. "A" represents the distributed main motor winding for phase a, "a" represents the sensing coil for phase a. In this case, the center line of the two coils is aligned. Similarly, sensing coils for phase b and phase c can be located. Each coil has an equal number of turns and one turn in this study.

Fig.5.5 shows a flux coil layout for the machine with 36 stator teeth and 4-pole rotor. The armature winding pitch is arranged such that the flux axes of the three stator phase windings are aligned along stator teeth. Relatively thin wire is used

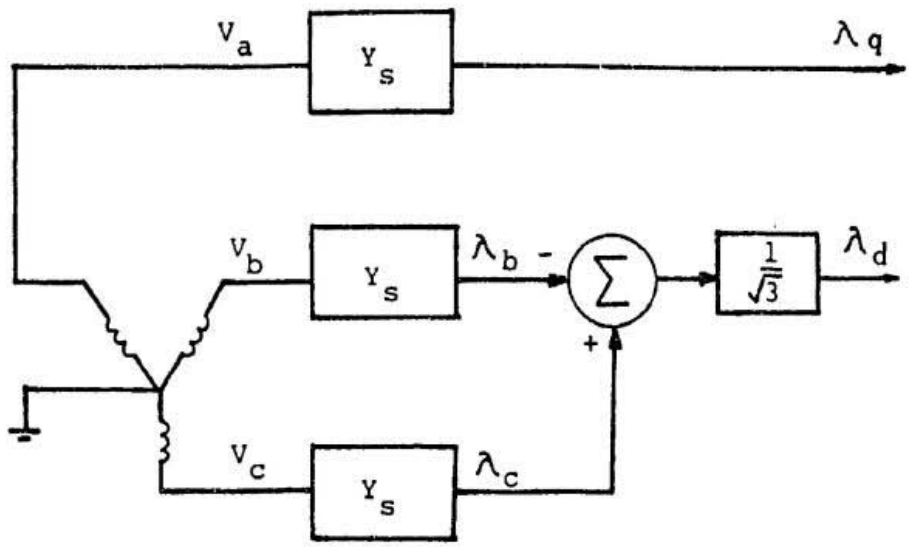

Figure 5.3: Implementation of the measurement realization

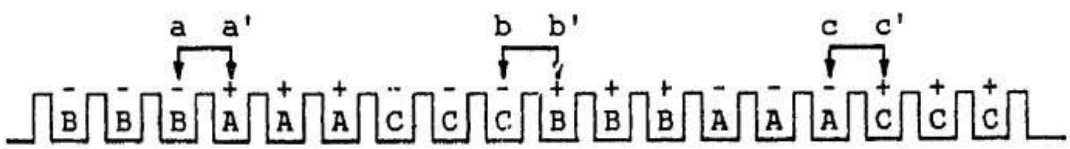

Figure 5.4: Search coil arrangement

for the search coil in this case, yet with sufficient strength to avoid breakage. Wire size approximately 30 AWG is the choice for this work. The d- and q-axes must be located first. The magnetic axis of the d-axis can be located by energizing the phase a winding with a small direct current. By counting forward in the direction of rotation by $S/2P$ tooth pitches the q-axis can be located. Once d- and q- axes are located, coils can be inserted into the motor according to Fig.5.5. In this figure, the voltage v_a, v_b and v_c are air gap voltages measured by three sensing coils and are transformed into ψ_a, ψ_b and ψ_c by integrating them, representing by 1/S. Three integrator coefficients are represented by K_a K_b and K_b respectively. The negative ψ_c come from ψ_c by use of a inverse circuit and is added with ψ_b to obtain d-axis flux. Since the q-axis is aligned with phase a, q-axis flux is obtained from ψ_a directly. In order to maintain accuracy in the flux measurement, high quality, lower noise and lower drift amplifiers are used to form the integrator. By choosing $R_f = R_i = 10k\Omega$, $C = 2.2\mu$, where R_f and C are the feedback resistor and capacitor respectively and R_i is the input resistor:

$$\begin{aligned} |\frac{\dot{V}_0}{\dot{V}_i}| &= \frac{A_v}{\sqrt{1^2 + (\frac{\omega}{\omega_0})^2}} \\ &\doteq \frac{A_v}{8.35} \\ &= \frac{1}{8.35} \\ &= K_a \end{aligned} \tag{5.12}$$

where $A_v = \frac{R_f}{R_i} = 1$, $\omega_0 = \frac{1}{R_f C} = 45.45\ rad.$ and $K_a = K_b = K_c$ for the three phases. Appendix IV shows the waveforms obtained from the search coils.

5.3.3 Measurement of Current Components

The d-q transformation for the current is similar to that shown earlier for the voltage equations and is given by:

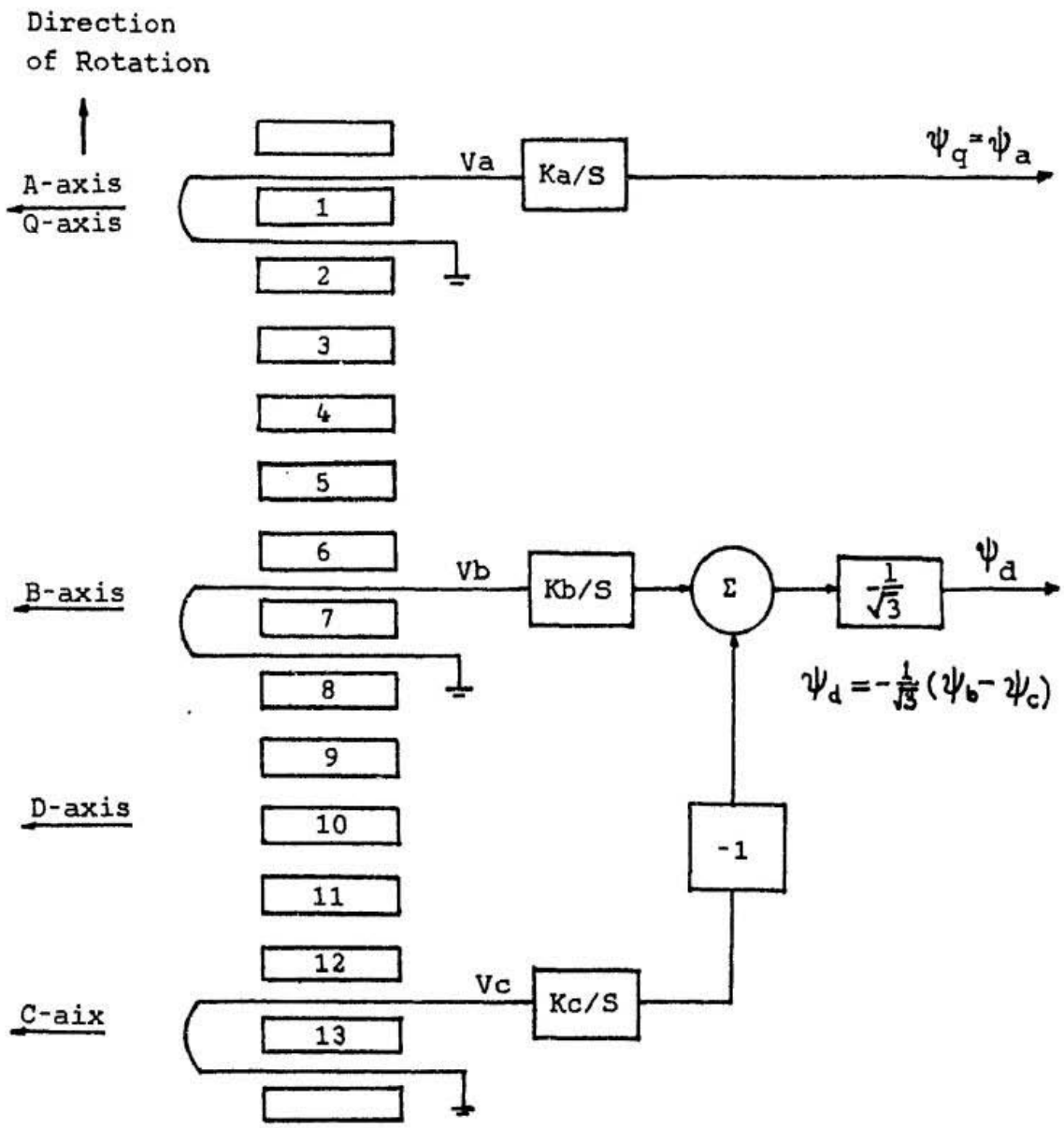

Figure 5.5: Flux coils arrangement using one coil per axis

$$\begin{bmatrix} i_q \\ i_d \\ i_0 \end{bmatrix} = \frac{2}{3} \begin{bmatrix} cos\theta & cos(\theta - 120^0) & cos(\theta + 120^0) \\ sin\theta & sin(\theta - 120^0) & sin(\theta + 120^0) \\ 0.5 & 0.5 & 0.5 \end{bmatrix} \begin{bmatrix} i_a \\ i_b \\ i_c \end{bmatrix} \tag{5.13}$$

Simplified as:

$$\begin{aligned} i_q &= i_a \\ i_d &= \frac{1}{\sqrt{3}}(i_c - i_b) \end{aligned} \tag{5.14}$$

Arrangement of current measurement is shown in Fig.5.6. Currents i_a, i_b and i_c can be measured by use of current transformer. Current transformer model LEM SA CH-1228 is used in this task. The summation circuit and integrator used in the current measurement is the same as those used for the voltage measurement. Waveforms of current components measured are also included in Appendix *IV*.

5.3.4 Calculation of Reactance

Since the flux waveform obtained from the search coils is nonsinusoidal, Fourier series analysis is used to calculate the fundamental component of the flux. The calculation consists of several steps as follows [37].

- to determine the coefficients of sine and cosine terms of the relevant Fourier series by means of approximate methods,
- to determine the value of the flux fundamental component,
- to determine I_d, I_q and calculate X_d and X_q.

The general Fourier series expression is given by:

$$f(x) = \frac{1}{2}a_0 + \sum_{n=1}^{\infty} a_n \cos nx + b_n \sin nx \tag{5.15}$$

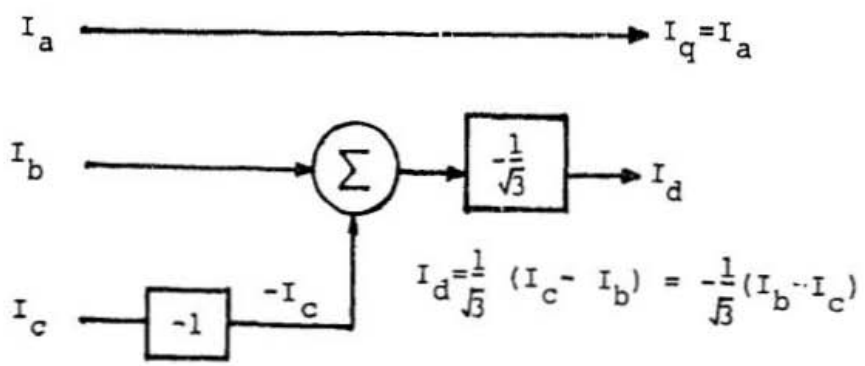

Figure 5.6: Measurement of current components

where a_0, a_n and b_n are the Fourier coefficients defined as:

$$\begin{aligned} a_0 &= \frac{1}{\pi}\int_0^{2\pi} f(x)\,dx \\ a_n &= \frac{1}{\pi}\int_0^{2\pi} f(x)\cos nx\,dx \\ b_n &= \frac{1}{\pi}\int_0^{2\pi} f(x)\sin nx\,dx \end{aligned} \tag{5.16}$$

It is known that approximate integration, which is equivalent to finding an area, can be performed by the application of the trapezoidal rule. In this study, twelve-point analysis is used. An example of determining coefficients (corresponding to the case when $I_a = 6.5A$) is presented below. The waveform obtained from the sensing coils is shown in Fig.5.7. Values of the ordinate for one cycle of a periodic waveform of period 2π are given in Appendix IV. It can be observed that for the flux waveform shown in Fig.5.7, $f(x) = f(x+\pi)$, also $f(x) = -f(x+\pi)$, i.e., the function contains odd harmonics only. Thus Fourier coefficients are calculated as follows.

To find a_1 (for ψ_a):

$$\begin{aligned} a_1 &= 2 \times \textit{mean value of } f(x)\cos x \textit{ over a period} \\ &= \frac{1}{6}\sum_{r=0}^{11} y_r \cos x_r \\ &= 2 \times \frac{1}{12}\textit{ sum of 12 ordinate} \\ &= 1.999 \end{aligned} \tag{5.17}$$

Finding all the coefficients by the procedure given in equation (5.17) gives the following results:

$a_1 = 1.9990$ $\qquad$ $b_1 = 29.927$

$a_3 = -1.283$ $\qquad$ $b_3 = 18.807$

$a_5 = -0.715$ $\qquad$ $b_5 = -7.311$

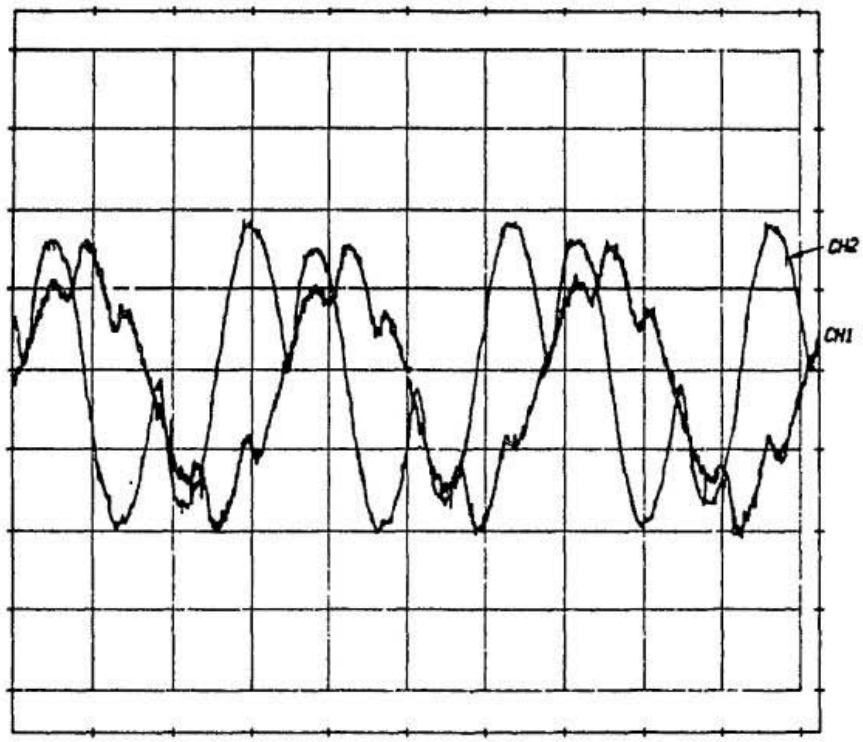

Figure 5.7: Flux waveform of I_a=6.5 A, ch1: ψ_d ch2: ψ_q

The fundamental component of the flux can be calculated after the Fourier coefficients are determined. It gives,

$$\begin{aligned} \psi_q &= \sqrt{\frac{1}{2}(a_1^2 + b_1^2)} / K \\ &= 21.21\, mwb \times 8.35 \\ &= 0.177\, wb \end{aligned} \tag{5.18}$$

ψ_d can be calculated the in same way:

$$\begin{aligned} \psi_d &= 21.7\, mwb \times 8.35 \\ &= 0.181\, wb \end{aligned} \tag{5.19}$$

Since current are sinusoidal components, its rms value can be determined simply. X_d and X_q are given from $X = \omega L = \omega \psi / I$, calculation of ψ_d and ψ_q for the load test is shown in Appendix *IV*. Recording the flux and the current components corresponding to each step load, the d-axis and q-axis reactance can be obtained and results are shown in Table 5.3 and Fig.5.8. The modified conventional test result is also included to present a comparison. Only a reasonable agreement between these two methods can be observed. The reason for this is due to the difficulty of separating the magnet and stator winding flux involved in the measurement of the search coil test. All the test methods and results will be discussed in the following section.

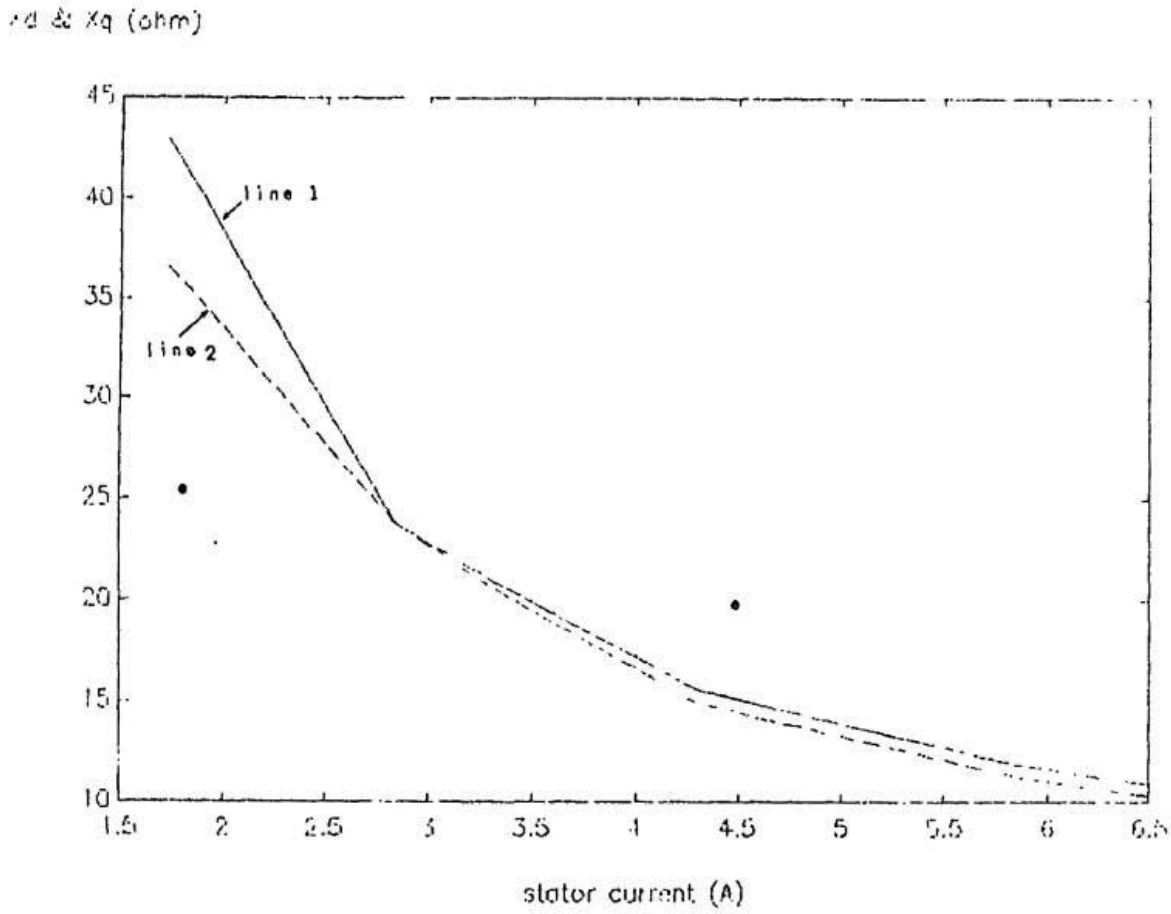

Figure 5.8: Results of search coil test: line 1–X_d line 2–X_q, symbol–modified conventional test

Table 5.3: Results of search coil test

I_a (A)	ψ_d (wb)	ψ_q (wb)	X_d (Ω)	X_q (Ω)
1.73	0.1789	0.1680	42.96	36.59
2.83	0.1676	0.1790	23.75	23.76
3.3	0.1778	0.1809	21.98	20.66
4.3	0.1617	0.1708	15.63	14.98
5.8	0.1440	0.1753	11.89	11.30
6.5	0.1812	0.1771	10.88	10.27

5.4 Discussion of Tests Results

Several test methods for determining the parameters of a P.M. synchronous motor have been presented and discussed in the preceding chapter and the preceding sections of this chapter. Emphasis there has been placed upon obtaining the three most significant parameters of the P.M. machine, namely the direct and quadrature axis reactances X_d and X_q as well the internal generated voltage E_i. Measurement of these parameters is difficult since the field excitation due to the permanent magnets cannot be removed and because the effects of the generated voltage and the direct axis reactance are always combined along the same axis and cannot be separated. Moreover, each of these parameters are shown to be load dependent and not constant as is often assumed. The following section is presented to discuss the various test results and to show the relative merit of each of the test methods presented.

As previously mentioned the effects of X_d and E_i are combined and the level of E_i is not independently controllable. In order to separate the effects of these two quantities the machine must be operated under conditions for which E_i or the effect of the reactance X_d goes to zero. Just such a condition exists when the direct-axis current is zero. One obvious operating point where this occurs is when the machine is being driven as an open circuit generator. The other is when the load is such that the torque angle is equal to the power factor angle. In each of these cases the value of E_i is easily measured with a voltmeter. Table 5.1 shows the results of these tests and also clearly shows the significant increase in E_i from no load to full load. Also shown in the table is the results obtained using the search coil simulation. The method was calibrated at near full load and shows good agreement with the only other measurable test condition.

Not only the generated voltage, but the axis reactances are also load dependent quantities which exhibit saturation characteristics. The inability to vary the field excitation renders the conventional tests inadequate for determining the axis reactances.

Table 5.4: Variation of generated voltage E_i

Condition	Measured value [V]	Computed from search coil simulation [V]
open circuit	118	118
zero d-axis current (near full load)	159.2	159.8

Several test methods for determining the value of X_d and X_q have been presented and are compiled together in Table 5.5 to show comparative results.

The modified conventional tests are not applicable for determining the values of X_q and give approximate values for the saturated and unsaturated d-axis reactance. The open and short circuit components used to determine X_d (sat.) $= E_0/I_{sc}$ are operating at different levels of saturation and the rms value of I_{sc} has a signifi- -at 3rd harmonic component. Overall, the results are reasonable and very easy to obtain. Since the flux linkage test is a static test, this gives another means for separating the the effects of E_i and X_d. Because there is no rotation there can be no magnet induced voltage, the test gives quite accurate results for the axis reactance quantities but requires a balanced bridge which is very hard to maintain in the balanced condition due to the thermal heating effect on the resistances. This effect is exacerbated at high current levels which are near or exceed the rated values. The search coil test involves flux quantities produced by both magnets and stator current while current quantity measured is produced by applied voltage only. It may results in abnormally high d-axis reactance values at unsaturation conditions. The load test provides reasonable agreement results with the other methods for the q-axis quantities but is in considerable disagreement for the high loaded d-axis reactance values. The equation used to compute the value

Table 5.5: Measurement of axis reactance

condition	parameter	method 1	method 2	method 3	method 4
unsaturated	X_d (Ω)	25.3	24.8	10	37
	X_q (Ω)	N/A	39	35	30.6
saturated	X_d (Ω)	20.5	18.8	14.8	90
	X_q(Ω)	N/A	23	32	23.2

- Method 1: Modified conventional test
- Method 2: Flux linkage test
- Method 3: Search coil test
- Method 4: Load test
- N/A: Not applicable

of X_d has a singular point which lies in the region where the loading is high thus the results are very sensitive to small changes in measured quantities. The load test requires a value for E_i in order to calculate the value of X_d which is a arbitrary way of separating the two effects along the d-axis excepting the operating point where d-axis current is zero. A summary of the test methods is is given in Table 5.6.

Table 5.6: Summary of the test methods

Method	Parameters obtained	Comments
Modified conventional test	E_0 and X_d	Good approximate results; easy to perform
Flux linkage test	X_d and X_q	Good results over full load range; hard to perform at high current levels
Search coil test	X_d and X_q	Reasonable results; some error for unsaturated value of X_d; both magnet and winding flux components present which are difficult to separate
Load test	X_d and X_q	Requires value for E_i; very sensitive to measurement error for some load condition; good result for X_q and indicates the variation of X_d at the full load range
Search coil simulation	E_i	Good result for a specific load operating point where d-axis current is zero

Chapter 6

CONCLUSIONS AND SUGGESTIONS

6.1 Conclusions

It is well known that the accurate prediction of the performance of the P.M. synchronous machines depends mainly on the accuracy of the evaluation of d-q axes reactance. The evaluation of d-q axes parameters of this kind of machine by using the test methods has been carried out in this thesis. The work is intended to determine axes reactances and internal generated voltage under load conditions.

A general introduction of the P.M. synchronous motor has been presented in Chapter 1, in which the comparison of the P.M. synchronous motor and conventional synchronous motor or induction motor was discussed. In Chapter 2, the standard tests for the conventional synchronous motor have been presented and the three characteristic features of the P.M. synchronous motor were discussed. The literature on the determination of P.M. synchronous motor parameters has also been reviewed from which the objective of this work is derived. The evaluation of the air gap fields of the P.M. synchronous motor has been developed in Chapter 3 which shows the air gap fields of the P.M. machine consists of both magnets fields and armature fields.

An analog simulation of the interaction of the field quantities in the air gap has been shown. As a result of the analog simulation, it has also been presented that torque angle of the P.M. motor can be measured by a digital electronic method instead of that from motor shaft. This provides a practical and accurate measurement of the torque angle. The influence of the armature reaction has been investigated and variation of the generated voltage under load condition has been presented in Chapter 1. It has been shown that the generated voltage is produced by a combination of the magnet and the armature components which contain a leakage factor. This leakage factor has significantly different values at different load conditions. Consequently, it results in change of generated voltage at loading. Furthermore, it results in the d-axis reactance varying with the load. A number of test methods for determining axes reactances under load conditions have been presented in Chapter 1 and Chapter 5. The result of the various methods has been discussed in last chapter.

In short, upon the examination of the thesis, the major contributions of this work are listed as follows:

- An analog simulation to verify the interaction of various components in the air gap of the P.M. machine has been presented. The air gap field model has been evaluated from configuration of the rotor and magnetic circuit of the machine. The analog simulation has been presented based on this air gap field model and the results of simulation have been shown that this air gap model provides a sufficient reasonable description for the actual air gap fields of the machine.

- A digital technique to measure the torque angle of the machine has been developed. In the load test, motor's torque angle must be measured in order to determine the steady-state performance of the machine. The technique presented in this work has brought several advantages for load test as compared with the existing method currently used. It is more convenient to carry out and has higher resolution of the measurement results. It makes a digital electronic

measurement possible and can be used in microprocessor-based measurement system and machine drive system where a fast-response digital measurement is required.

- The armature reaction influence on generated voltage has been analyzed and the saturated value of the generated voltage has been experimentally determined. It has been shown that the saturated value of the generated voltage is not equal to that of the open-circuit value. Upon examination of the phasor diagram of the machine and the flux linkage paths of the rotor under different load conditions, it has been observed that applied voltage results in a magnetizing (demagnetizing) current during the light (heavy) loading. Therefore, the armature reaction results in a significant increase of the generated voltage over the range of loads. The investigation of the variation of the generated voltage at loading has significant meaning in determining the saturated value of the axes reactances by use of modified conventional test and load test. By using the saturated value of the generated voltage, the modified conventional test has presented a better approximate saturated value of the d-axis reactance than that by using the open circuit voltage. Secondly, for the load test, the negative values of the d-axis reactance do not appear in any range of the loads. This is consistent with the statement that the negative values for X_d are entirely consequent upon the assumption of constant E_0.

- Several test approaches to determine axes reactances have been presented and discussed. Each of the test methods is compared with respect to their usefulness and range of validity.

6.2 Suggestions for Further Study

The thesis submitted here is focused on the test methods used to determine the P.M. synchronous motor parameters. Thus, further work to be done should include:

- Measurement of the steady state performance of the machine, from which the torque vs torque angle characteristic can be obtained experimentally.
- Determination of the generated voltage over the entire region of loads by digital simulation or finite-element techniques.
- Prediction of the steady state performance of the machine based on the two axis reactances determined by different test methods. Subsequently, correlation of the measurement results and calculation results.

References

[1] T. Sebastian, " Steady State Performance Variable Speed Permanent Magnet Synchronous Motors ", Ph.D Thesis, University of Toronto, Canada. 1986

[2] T.A. Little, " Design and analysis of permanent magnet synchronous motor ", M. Eng. Thesis, Memorial University of Newfoundland, Canada, 1984

[3] Alexander Levrar and Enrico Levi, " Deign of Polyphase Motors with PM Excitation ", IEEE. Trans. on Magnetics, Vol. MAG-20, No.3, May, 1984, pp.507-515

[4] T.J.E. Miller, T.W.Neumann, and E.Richter, "A permanent magnet excited high efficiency synchronous motor with line-start capability ", IEEE IAS Annual Meeting, Mexico city, Oct. 1983, pp. 455-461

[5] P. Zimmerman, "Electronically commutated dc feed drives for machine tools", Drives Contr. Int. Vol. 2, pp. 13-20, Oct./Nov. 1982

[6] T.W. Neumann and R.E. Tompkins,"Line start motors designed with Nd-Fe-B permanent magnets", in Proc. 8th Int. Workshop Rare-Earth Magnets, Ohio. USA, May 1985, pp.77-89

[7] B.K. Bose, " A High Performance Inverter-Fed Drive System of An Interior Permanent Magnet Synchronous Machine ". IEEE ISA Annual Meeting, Atlanta, GA, USA, Oct. 1987, pp.269-276

[8] T.A. Little, M.A. Rahman, " Effect of High Coercive Force on Stating Performance of Permanent Magnet Motors " .7th International Workshop on Rare Earth Cobalt Magnet and their Applications . Beijing, China, Sept. 1983, pp.29-36

[9] M.A. Rahman, A.M. Osheiba, " Effect of Parameter Variations on The Performance of Permanent Magnet Motors ". IEEE IAS Annual Meeting, Denver, Co., USA, Sept.28-Oct.3, 1986, pp.787-793

[10] Thomas M. Jahns, Gerald B. Kliman, Thomas W. Neumann, " Interior Permanent-Magnet Synchronous Motors for Adjustable-Speed Drives ", IEEE Trans. on Ind. Appl. IA-22, No. 4, July/August, 1986, pp.738-747

[11] T.J.E. Miller, " Synchronization of Line-Start Permanent-Magnet AC Motors ", IEEE Trans. on Power App. and Sys. Vol.PAS-103, No.7, July, 1984, pp.1822-1828

[12] E. Richter, " Permanent Magnet Motors Final Report ", Oak Ridge National Laboratory report, ORNL/SUB/17452/1. DEC. 1983

[13] M.A. Jabbar. "Analysis of The Performance of A Permanent-Magnet A.C. Machine " Ph.D Thesis, Southampton University, Hants. S09 5NH. England, June 1977

[14] "Test Procedures for Synchronous Machines" IEEE Std. 115-1983

[15] Leander W. Matsch and J. Derald Morgan, "Electromagnetic and Electromechanical Machines" (book), New York, IEP, 1977

[16] Mulukutla S. Sarma, "Synchronous Machine (Their Theory, Stability, and Excitation Systems)", Gordon and Breach, Science Publishers Inc. New York, NY, 1979

[17] E. Richter and T.W. Neumann, " Synchronous machine designs using different types of permanent magnets ", Paper No.1-1, Fifth Int. Workshop on Rare Earth-Cobalt Permanent Magnets and Their Applications; Roanoke, VA, June 1981, pp.1-27

[18] V.B. Honsinger, " Performance Polyphase Permanent Magnet Machines ", IEEE Trans. Vol. PAS-99, No.4, July/Aug.1980, pp.1510-1516

[19] T.J.E. Miller, " Methods for Testing Permanent Magnet Polyphase A.C. Motors ", IEEE IAS Cof. Record No. 81ch1678-2, 1981, pp.494-499

[20] Fitzgerald, A.E., Kingsley, C.Jr., Kusko, A., "Electric Machinery", (book), McGraw-Hill, New York, NY, 1971

[21] V.B. Honsinger, " The Fields and Parameters of Interior Type A.C.Permanent Magnet Machines ", IEEE Trans. Vol. PAS-101, No.4, 1982, pp.867-875

[22] A. Hameed, K.J. Binns, A. Vandenput, W. Geysen," The Finite-Element Computation of The Field in A Permanent Magnet Machine", Electrical Machines and Converters, Elsevier Science Pulishers B.V. (North-Holland)/IMACS 1984, pp. 107- 111.

[23] K. Miyashita, S. Yamashita, S. Tanabe. T. Shimozu, H. Sento, "Development of A High Speed 2-pole Permanent Magnet Synchronous Motor", IEEE Trans. Power App. Sys. Vol. PAS-99, No.6, 1980, pp.2175-2183.

[24] K.J. Binns, C.P. Riley, T.W.Wong, " Some Design Aspects of High-Output Permanent Magnet Synchronous Machines with Non-Radial Magnets ", Second Int. Conf. on Electrical Machines Design and Applications (Conf. Publ. No.254) IEE 1985, London, England, 17-19, Sept. 1985

[25] Nady Boales, " Field Analysis of P.M. Synchronous Machines with Buried Magnet Rotor ", Intl. Conf. on Electrical Machines, Munchen, Germany, Sept. 1980, pp.1063-1066

[26] K.J. Binns, M.A. Jabbar, G.E. Parry, " Choice of Parameters in the Hybrid Permanent Magnet Synchronous Motor ", Proc. IEE, Vol.125(8), Aug.1979, pp.741-744

[27] K.J. Binns, M.A. Jabbar, " High-Field Self-Starting Permanent Magnet Synchronous Motors ", IEE Proc. B, Electric Power Appl., 1981, 128(3), pp.157-160

[28] M.A. Rahman, T.A. Little, G.R. Slemon, " Analytical Models for Interior-Type Permanent Magnet Synchronous Motors ", IEEE Trans. on Magnetics, Vlo. MAG-21, No.5, Sept. 1985

[29] C.V. Jones,"The Unified Theory of Electrical Machines", Butterworths, London, 1967

[30] S.I. Ahson, M.H. Ali, " A Microprocessor-Based Scheme for Torque-Angle and Speed Measurement ", IEEE Trans. on Industrial Electronics, Vol.IE-34, No.2, May,1987, pp.135-138

[31] T.K.M. Babu, Denis O'kelly, " A Microprocessor-Based Load Angle Measurement System ", IEEE Trans. on Industrial Electronics, Vol.IE-34, No.2, May, 1987, pp.129-134

[32] S.F. Gorman, C. Chen, J.J. Cathey, "Determination of Permanent Magnet Synchronous Motor Parameters for Use in DC Brushless Motor Drive Analysis", IEEE Trans. on Energy Conversion, Vol.3, No.3, 1988, pp.674-681

[33] T.A. Lipo,"Flux Sensing and Control of Static AC Drives By the Use of Flux Coils", IEEE Trans. on Magnetics,Vol.MAG-13,No.5, Sept.1977, pp.1403-1408

[34] A.B. Plunkett."A Current-Controllled PWM Transistor Inverter Drive",IEEE IAS Annual Meeting, Conf. Record, Clevel and Ohio, USA, Sept.30-Oct.4, 1979, pp.785-792

[35] R.H. Park, "Two-Reaction Theory of Synchronous Machine- Generalized Method of Analysis-Part I, " AIEEE Trans., Vol.48, July,1929, pp. 716-727.

[36] B.K. Bose,"Power Electronics And AC Drives", (book), Prentice-Hall, Englewood Cliffs, NJ, 1986

[37] K.A. Stroud,"Fourier Series and Harmonic Analysis", (book), Stanley Thornes, (Publishers) Ltd. 1984

Appendix I

Circuits of Analog Simulation

Figure I.1: Analog simulation circuits

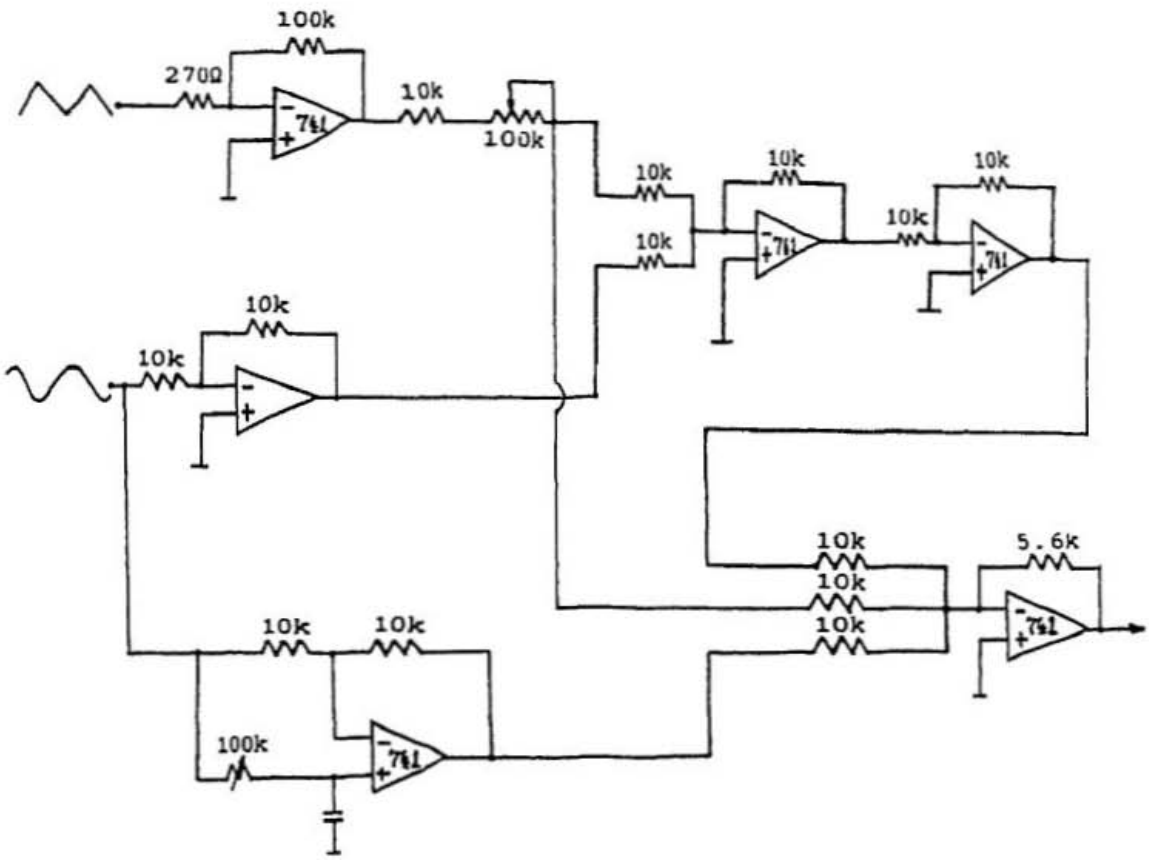

Appendix II

Circuits of Digital Measurement of Motor Torque Angle

Figure II.1: Circuits of digital measurement of motor torque angle

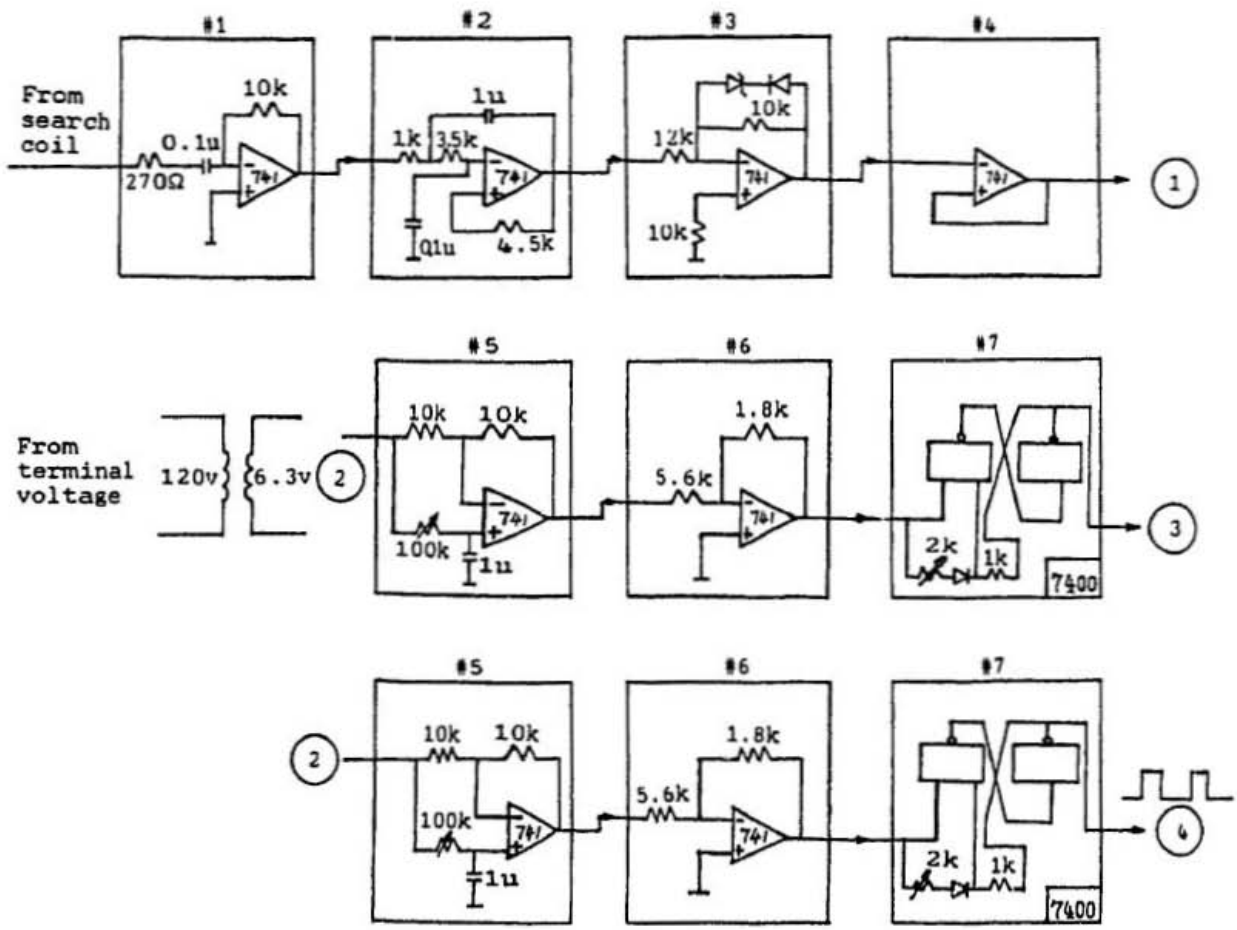

Figure II.2: Circuits of digital measurement of motor torque angle-cont'd

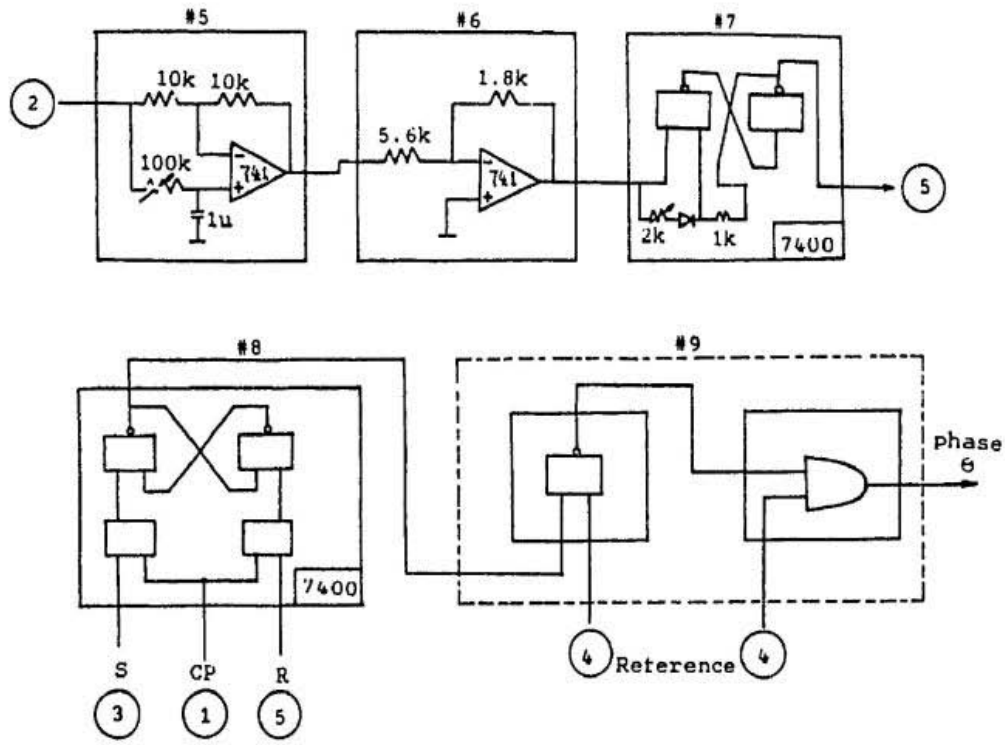

#1: Differentiator
#2: Filter
#3: Clipper
#4: Voltage follower
#5: Phase shifter
#6: Attenuator
#7: Schmitt trigger
#8: Flip-flop
#9: Phase detector

#1: Differentiator
#2: Filter
#3: Clipper
#4: Voltage follower
#5: Phase shifter
#6: Attenuator
#7: Schmitte trigger
#8: Flip-flop
#9: Phase detector

Appendix III

Rotor Geometry and Parameters

Figure III.1: Rotor magnet geometry for calculating leakage factor a) dimensions b) flux paths

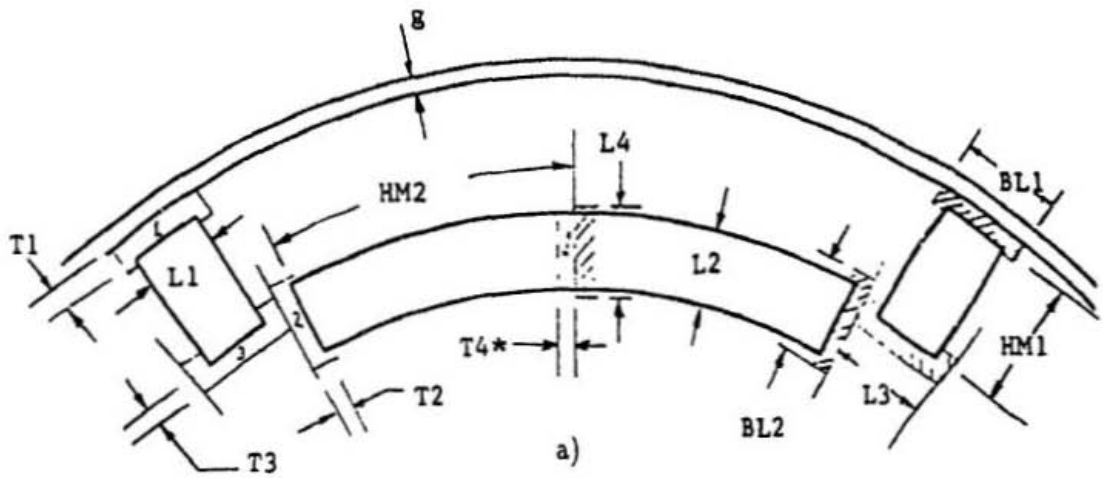

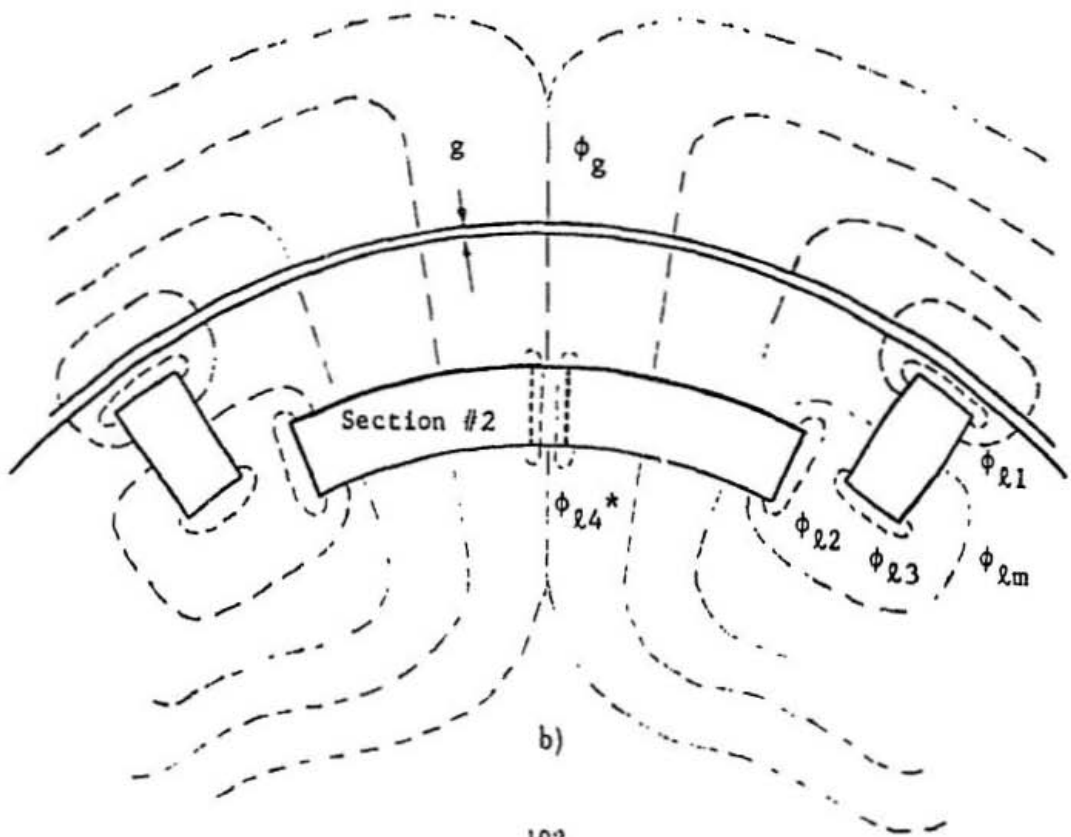

Figure III.2: Machine and magnet parameters for calculating leakage factor

Symbol	Description	
Motor Parameters:		
G	Effective air gap length including Carter's coefficient and saturation	0.0330
D	Rotor outside diameter	6.849
LS	Length of rotor core	7.620
Magnet Parameters:		
HM1	Dimension of magnet section 1 perpendicular to useful flux	0.9906
HM2	Dimension of magnet section 2 perpendicular to useful flux	2.680
L1	Length of magnet #1 in direction of flux	0.559
L2	Length of magnet #2 in direction of flux	0.508

Symbol	Description	
Rotor Geometry:		
BL1	Length of leakage bridge above magnet section 1	0.565
BL2	Length of leakage bridge above magnet section 2	0.553
L3	Length of leakage bridge under magnet section 1	0.085
L4	Length of leakage bridge in middle of magnet section 2	0.553
T1	Thickness of bridge corresponding to BL1	0.039
T2	Thickness of bridge corresponding to B12	0.104
T3	Thickness of bridge #3	0.556
T4	Thickness of bridge #4	0.124

Appendix IV

Calculation of Reactances

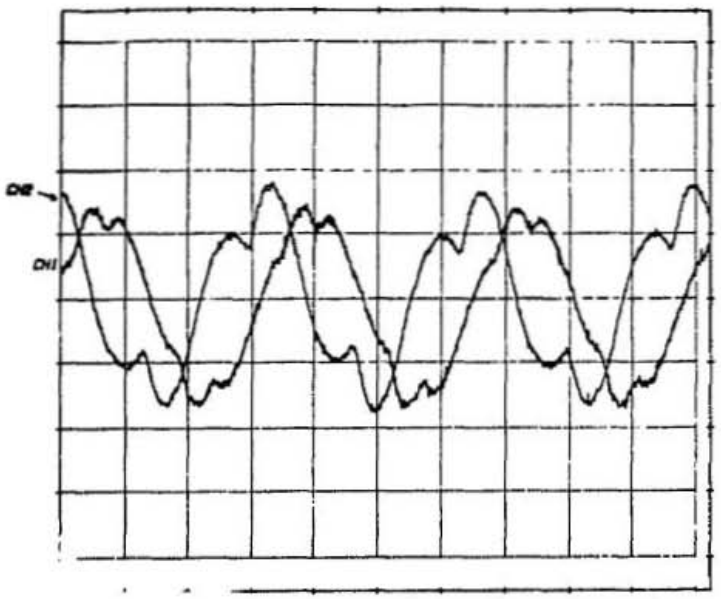

Figure IV.1: Flux component: $I_a = 2.85\,A$ ch1: ψ_{d2} ch2: ψ_{q2}

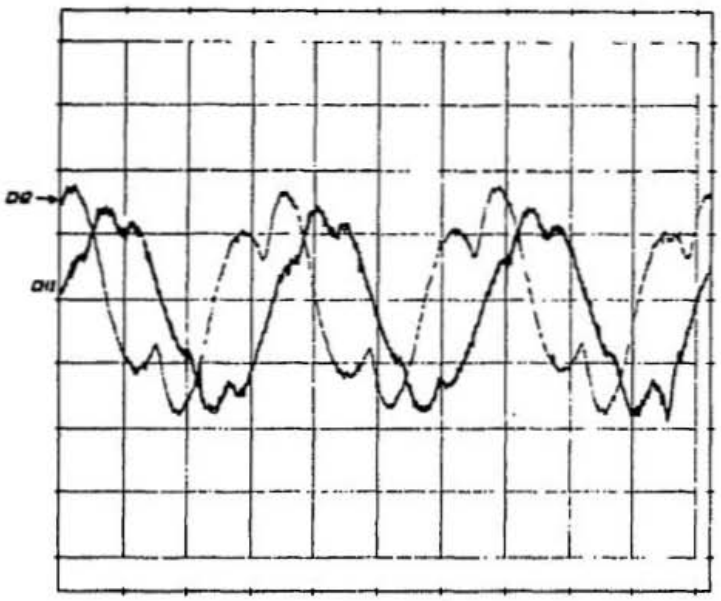

Figure IV.2: Flux component: $I_a = 3.3\,A$ ch1: ψ_{d3} ch2: ψ_{q3}

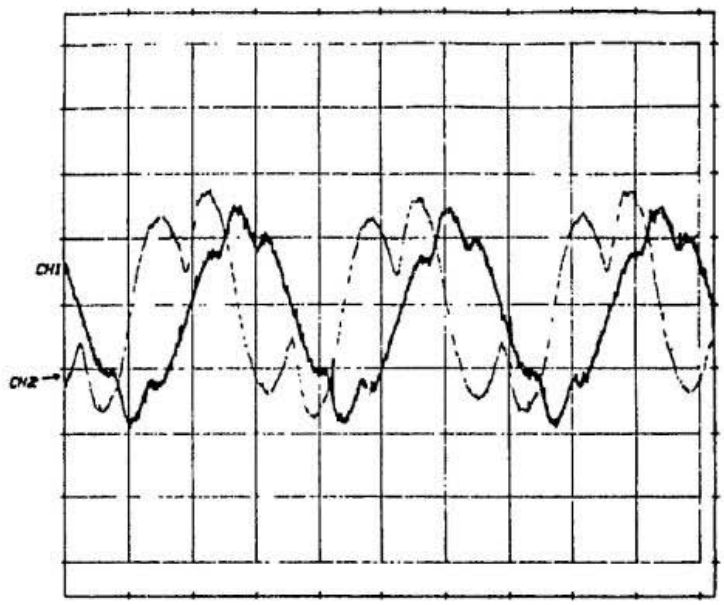

Figure IV.3: Flux component: $I_a = 4.3\,A$ ch1: ψ_{d4} ch2: ψ_{q4}

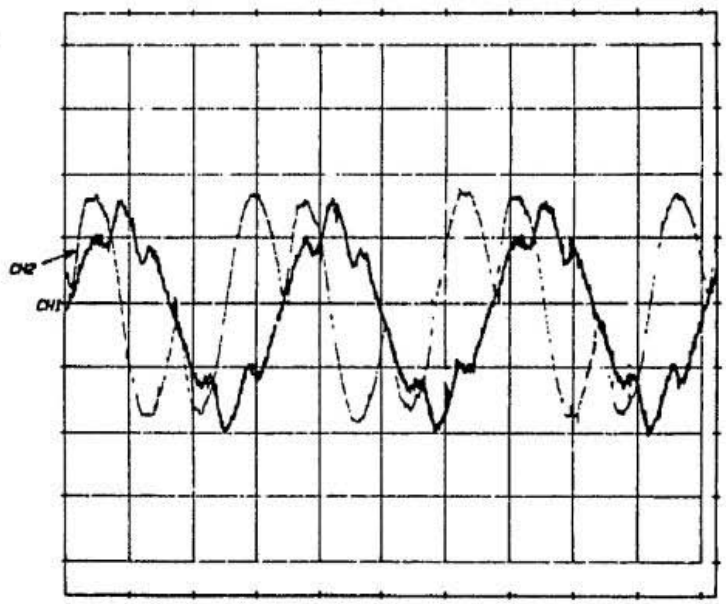

Figure IV.4: Flux component: $I_a = 5.8\,A$ ch1: ψ_{d5} ch2: ψ_{q5}

Table IV.1: Values of the ordinate for d-axis flux of one cycle

x (^{0})	ψ_{d1} (mwb)	ψ_{d2} (mwb)	ψ_{d3} (mwb)	ψ_{d4} (mwb)	ψ_{d5} (mwb)	ψ_{d6} (mwb)
0.0	0.0	0.0	0.0	0.0	0.0	0.0
30.0	15.7	12.2	14.25	14.78	11.5	16.23
60.0	26.0	24.4	23.95	19.3	18.0	23.7
90.0	31.6	27.8	30.45	31.4	29.75	34.2
120	26.0	26.1	24.6	20.95	17.25	23.7
150	12.8	14.9	16.5	17.2	14.25	17.4
180	0.0	0.0	0.0	0.0	0.0	0.0
210	-15.7	-12.2	-14.25	-14.78	-11.5	-16.23
240	-26.0	-24.4	-23.95	-19.3	-18.0	-23.7
270	-31.6	-27.8	-30.45	-31.4	-29.75	-34.2
300	-26.0	-26.1	-24.6	-20.95	-17.25	-23.7
330	-12.8	-14.9	-16.5	-17.2	-14.25	-17.4

Note, ψ_{d1}, ψ_{d2} .... ψ_{d6} and ψ_{q1}, ψ_{q2},...ψ_{q6} correspond to the amplitude of the d-axis and q-axis flux waveform when the stator current is $1.73\,A$, $2.85\,A$ ... $6.5\,A$ respectively.

Table IV.2: Values of the ordinate for q-axis of one cycle

x (^{0})	ψ_{q1} (mwb)	ψ_{q2} (mwb)	ψ_{q3} (mwb)	ψ_{q4} (mwb)	ψ_{q5} (mwb)	ψ_{q6} (mwb)
0.0	0.0	0.0	0.0	0.0	0.0	0.0
30.0	11.6	16.1	17.6	21.75	28.1	30.65
60.0	23.17	19.1	21.2	26.8	32.75	36.05
90.0	30.15	25.0	20.3	11.57	6.0	5.53
120	25.2	33.9	35.3	31.45	31.1	28.85
150	14.85	22.2	25.6	27.25	27.5	29.5
180	0.0	0.0	0.0	0.0	0.0	0.0
210	-11.6	-16.1	-17.6	-21.75	-28.1	-30.65
240	-23.17	-19.1	-21.2	-26.8	-32.75	-36.05
270	-30.15	-25.0	-20.3	-11.57	-6.0	-5.53
300	-25.2	-33.9	-35.3	-31.45	-31.1	-28.85
330	-14.85	-22.2	-25.6	-27.25	-27.5	-29.5

Calculations are given below:

1). $I_a = 1.73\,A$

d-axis: a_1=0.837 b_1=30.294 I_d=1.57 A ψ_d=0.1789 wb

q-axis: a_1=−1.276 b_1=28.422 I_q=1.73 A ψ_q=0.1678 wb

2). $I_a = 2.85\,A$

d-axis: a_1=−1.063 b_1=28.361 I_d=2.66 A ψ_d=0.16757 wb

q-axis: a_1=−4.228 b_1=30.016 I_q=2.85 A ψ_q=0.17897 wb

3). $I_a = 3.3\,A$

d-axis: a_1=−2.071 b_1=30.049 I_d=3.05 A ψ_d=0.1778 wb

q-axis: a_1=−4.659 b_1=30.277 I_q=3.3 A ψ_q=0.1809 wb

4). $I_a = 4.3\,A$

d-axis: a_1=−0.999 b_1=27.373 I_d=3.9 A ψ_d=0.1617 wb

q-axis: a_1=−2.363 b_1=28.839 I_q=4.3 A ψ_q=0.1708 wb

5). $I_a = 5.8\,A$

d-axis: a_1=−0.669 b_1=24.384 I_d=4.57 A ψ_d=0.1440 wb

q-axis: a_1=0.488 b_1=29.691 I_q=5.8 A ψ_q=0.1753 wb

6). $I_a = 6.5\,A$

d-axis: a_1=−0.338 b_1=30.688 I_d=6.28 A ψ_d=0.1812 wb

q-axis: a_1=1.999 b_1=29.927 I_q=6.5 A ψ_q=0.1771 wb

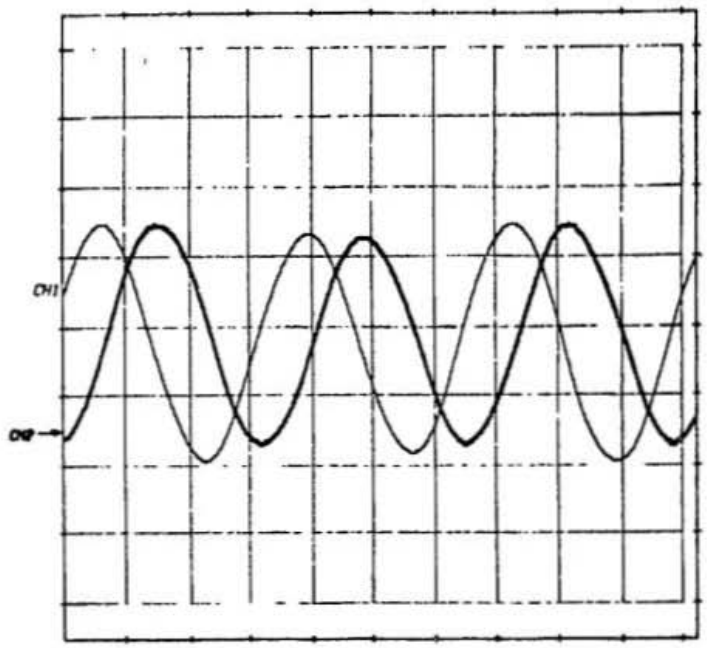

Figure IV.5: Current component: $I_a = 2.85\,A$ ch1: I_{q2} ch2: I_{d2}

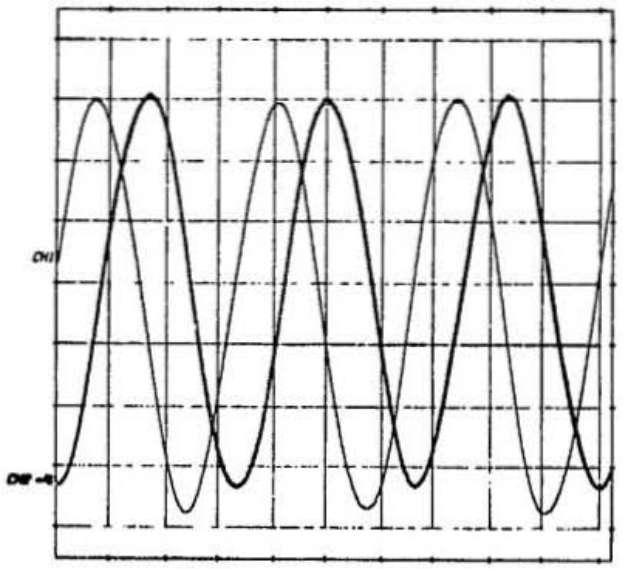

Figure IV.6: Current component: $I_a = 5.8\,A$ ch1: I_{q5} ch2: I_{d5}